Author Manuscript

Author Manuscript

Author Manuscript

Author Manuscript

HHS Public Access

Author manuscript

Ann Biomed Eng. Author manuscript; available in PMC 2015 April 22.

Published in final edited form as:

Ann Biomed Eng. 2011 August ; 39(8): 2223–2241. doi:10.1007/s10439-011-0321-6.

Integrin β4 Signaling Promotes Mammary Tumor Cell Adhesion to Brain Microvascular Endothelium by Inducing ErbB2-mediated Secretion of VEGF

Jie Fan[1,2], **Bin Cai**[1], **Min Zeng**[1], **Yanyan Hao**[3], **Filippo G. Giancotti**[#3], and **Bingmei M. Fu**[#1]

[1]Department of Biomedical Engineering, The City College of the City University of New York, New York, NY 10031

[2]Key Laboratory for Biomechanics and Mechanobiology of Ministry of Education School of Biological Science and Medical Engineering, Beihang University, Beijing 100191, China

[3]Cell Biology Program, Sloan-Kettering Institute for Cancer Research, Memorial Sloan-Kettering Cancer Center, New York, NY 10021

[#] These authors contributed equally to this work.

Abstract

Prior studies have indicated that the β4 integrin promotes mammary tumor invasion and metastasis by combining with ErbB2 and amplifying its signaling capacity. However, the effector pathways and cellular functions by which the β4 integrin exerts these effects are incompletely understood. To examine if β4 signaling plays a role during mammary tumor cell adhesion to microvascular endothelium, we have examined ErbB2-transformed mammary tumor cells expressing either a wild-type (WT) or a signaling-defective form of β4 (1355T). We report that WT cells adhere to brain microvascular endothelium *in vitro* to a significantly larger extent as compared to 1355T cells. Interestingly, integrin β4 signaling does not exert a direct effect on adhesion to the endothelium or the underlying basement membrane. Rather, it enhances ErbB2-dependent expression of VEGF by tumor cells. VEGF in turn disrupts the tight and adherens junctions of endothelial monolayers, enabling the exposure of underlying basement membrane and increasing the adhesion of tumor cells to the intercellular junctions of endothelium. Inhibition of ErbB2 on tumor cells or the VEGFR-2 on endothelial cells suppresses mammary tumor cell adhesion to microvascular endothelium. Our results indicate that β4 signaling regulates VEGF expression by the mammary tumor cells thereby enhancing their adhesion to microvascular endothelium.

Keywords

intercellular junctions; ZO-1; VE-cadherin; endothelial permeability; laminin-5; ErbB2; endothelial VEGF receptor

Corresponding author, (212)-650-7531, (212)-650-6727 (fax), fu@ccny.cuny.edu.

Author Manuscript Author Manuscript Author Manuscript Author Manuscript

INTRODUCTION

Despite the widespread recognition of metastasis as a critical component in tumor malignancy, very little has been learned about the mechanisms governing two of the critical steps in tumor metastasis, tumor cell adhesion to the microvasculature and extravasation into the stroma of the target organ. The integrins are a family of signaling and cell adhesion receptors, which attach cells to the extracellular matrix (ECM) and in some cases to other cells, and cooperate with growth factor and cytokine receptors to regulate cell behavior [14, 33]. Signals elicited by integrins enable tumor cells to survive, proliferate, and migrate independently of positional constrains [14, 15, 18], but the specific contributions of integrins to the arrest and extravasation stages of metastasis are not well defined.

The α6β4 integrin (here referred to as the β4 integrin) is a laminin-5 receptor and was originally described as a "tumor-specific" protein, because of its apparent upregulation in multiple metastatic tumor types, including breast cancers [13]. The β4 integrin is unique among integrins, because the cytoplasmic portion of the β4 subunit is 1017 amino-acid-long and possesses distinctive adhesive and signaling functions [13]. Upon binding of the ectodomain of β4 to the basement membrane protein laminin-5, the cytoplasmic portion of β4 interacts with the keratin cytoskeleton to promote the assembly of hemidesmosomal adhesions [23]. In addition, β4 activates intracellular signaling autonomously as well as by associating with multiple receptor tyrosine kinases (RTKs), including the EGFR, ErbB2, Met, and Ron [14, 16, 25]. Mice carrying a knock-in mutation that deletes the C-terminal portion of β4, including all major tyrosine phosphorylation sites, do not display skin fragility or other adhesion deficiencies, because the mutant integrin retain the ability of mediating the assembly of hemidesmosomes. However, they exhibit defective wound healing and fail to support effective tumor angiogenesis, suggesting that β4 signaling regulates wound repair and the invasive phase of angiogenesis [16, 27, 39].

The gene encoding the RTK ErbB2 (HER2) is amplified in 25-30% of breast cancers [35]. To examine the role of integrin β4 signaling in ErbB2-mediated mammary tumorigenesis, we have previously introduced a targeted deletion of the β4 signaling domain in MMTV-Neu mice[16]. MMTV-Neu mice carry an activated form of ErbB2 driven by a mouse mammary tumor virus (MMTV) promoter and develop mammary tumors [26] characterized by a gene-expression signature similar to that of human tumors carrying amplification of the HER2 locus [3]. Deletion of the β4 signaling domain delayed mammary tumor onset and inhibited primary tumor growth. The tumors arising in mutant mice were significantly more differentiated histologically as compared to control tumors. In addition, primary tumor cells expressing signaling-defective β4 displayed a reduced proliferative rate and invasive ability and underwent apoptosis when deprived of matrix adhesion. Finally, upon injection in the tail vein of nude mice, the mammary tumor cells expressing mutant β4 exhibited reduced ability to metastasize to the lung[16]. We did not however examine the mechanisms by which integrin β4 signaling promotes metastasis.

The endothelial layer that separates the bloodstream from the interstitial matrix of metastatic target organs acts as a formidable barrier to the extravasation of tumor cells under normal conditions [21]. A reasonable model posits that tumor cell-intrinsic proclivities, such as high-

Author Manuscript Author Manuscript Author Manuscript Author Manuscript

level expression of cell adhesion receptors for endothelial ligands and local secretion of matrix-degrading enzymes, conspire with local deficiencies in the integrity of the microvasculature to enable a small percentage of circulating tumor cells to arrest and extravasate at metastatic sites [7, 28, 38]. Recently, it has been shown that ectopic administration of vascular endothelial growth factor (VEGF), which is secreted by many tumor cells [32], enhances the adhesion and transmigration of human breast cancer MDA-MB-231 cells across a monolayer of human brain microvascular endothelial cells under a static condition *in vitro* [21]. In addition, VEGF enhances the adhesion of malignant MDA-MB-435 cells to intact rat mesenteric microvessels under flow *in vivo* [11, 34]. Although the role of integrin signaling in regulating VEGF expression has remained largely unexplored, Chung et al. [8] have proposed that the β4 integrin can enhance translation of the mRNA encoding VEGF, generating an autocrine loop that sustains their survival under stress.

Therefore, the objective of our study was to examine the role of β4 signaling in mammary tumor cell adhesion to microvascular endothelium, which is one of the critical steps during tumor metastasis. Using an *in vitro* cultured cell monolayer system, we quantified the adhesion of ErbB2-transformed mammary carcinoma cells expressing wild-type or signaling-defective β4 as well as their normal counterpart to brain microvascular endothelium (bEnd3). We also examined whether β4 signaling affects tumor cell adhesion to laminin-5, an ECM ligand of β4 integrin. Finally, because secretion of VEGF by tumors can enhance tumor cell adhesion, we examined whether integrin β4 signaling controls the expression of VEGF. Our results reveal that the β4 signaling cooperates with ErbB2 to induce tumor cells to secrete VEGF, which locally disrupts endothelial junctions and enhances exposure of underlying basement membrane to promote tumor cell adhesion to the intercellular junctions of microvascular endothelium.

MATERIALS AND METHODS

Solutions and reagents

Mammalian Ringer solution with 10 mg/ml BSA (1%BSA) (Sigma, A4378) [11] was used in both the adhesion assay and permeability measurement. All the materials used in making the Ringer solutions were purchased from Sigma (ST. Louis, MO) as well as the FITC-labeled BSA (MW~67kD, A9771). PBS was from Mediatech Inc. (Manassas, VA). 4′, 6-diamidino-2-phenylindole (DAPI) was from Invitrogen (Carlsbad, CA) Human recombinant VEGF165 and VEGF receptor (KDR/Flk-1) inhibitor, SU-1498, were obtained from Peprotech (Rocky Hill, NJ) and Alomone labs (Jerusalem, Israel), respectively. Iressa [25] was obtained from the Memorial Sloan-Kettering Cancer Center (MSKCC) Pharmacy. Both anti-human β4 (N-terminal) and anti-mouse β4 (C-terminal) antibodies were obtained from the Antibody Core Facility of MSKCC. Antibody against mouse integrin α6 subunit was from BD Pharmingen (San Diego, CA); monoclonal antibody against laminin-5 was from Santa Cruz Biotech (Santa Cruz, CA); rabbit antibodies against mouse ZO-1 and VE-cadherin were from Invitrogen (Carlsbad, CA). For hemidesmosome immunostaining, the monoclonal antibody 3E1 against the extracellular portion of β4 integrin[37], and the polyclonal antibody against the hemidesmosomal marker Bullous Pemphigiod Antigen 180 kDa (BPAG-1), were obtained from Millipore (Billerica, MA), as was laminin-5 for *in vitro*

Author Manuscript Author Manuscript Author Manuscript Author Manuscript

adhesion assays. The anti-β-actin antibody was from Sigma and a non-specific anti-mouse IgG was from GenScript (Piscataway, NJ).

Cell culture

The β4 wild type (WT) and β4 signaling defect (1355T) ErbB2-transformed mammary carcinoma cells were obtained from the MSKCC. Generation of these transformed tumor cells has been described in Guo et al. (2006) [16]. These cells were cultured in Dulbecco's modified eagle's medium/Nutrient mixture F-12 Ham (DMEM/F-12) supplemented with 10% fetal bovine serum, nonessential amino acids, 1 μg/ml hydrocortisone, 10^{-9} M choleratoxin and 10 μg/ml insulin. The mouse normal mammary gland epithelial cells (NMuMG) and mouse brain microvascular endothelial cells (bEnd3) (ATCC, Manassas, VA) were cultured in DMEM/F-12 with 10% fetal bovine serum, 2 mM L-glutamine, 50 U/ml penicillin and 50 μg/ml streptomycin. All the cells were fed with fresh medium every two days and maintained in 5% CO_2 at 37°C.

Western blot

For determining the β4 integrin expression, WT, 1355T and NMuMG cells were lysed in lysis buffer (0.1 M Tris at pH 8.0, 1% SDS and 10% Glycerol) and were subjected to immunoblotting with anti-β4 and anti-β-actin antibodies.

VEGF ELISA

To determine the amount of VEGF secretion, 1 ml of WT, 1355T cells suspension (6×10^5/ml) in 1% BSA was added into each well with confluent bEnd3 monolayer and incubated under 5% CO_2, 37°C for 15 min, 1 hr, 2 hr and 6 hr for the co-culture adhesion. Same amount of WT or 1355T cells were placed into a blank well for the same periods for the mono-culture condition. One ml of 1% BSA was added to the bEnd3 monolayer as a sham control. At each time point, 900 μl of the culture medium from each well was collected; centrifuged and 500 μl supernatant of each sample was collected and kept frozen until analysis. VEGF concentration of each sample was determined using mouse VEGF ELISA kit (Invitrogen, #KMG0111).

Iressa treatment

WT or 1355T cells were seeded in each well at a density of 2×10^5/ml, incubated at 37°C overnight, and in serum free medium for 24 hr. Then the cells were treated with 10 μM Iressa for 1 hr, 6 hr, and 12 hr. After the treatment, the supernatant of each well was collected for the VEGF ELISA assay as described above, while the cells were immediately transferred for the quantitative RT-PCR.

Quantitative RT-PCR

A standard GAPDH based quantitative RT-PCR protocol was performed. Total RNA was extracted from both control and 10 μM Iressa treated WT and 1355T cells by using the RNeasy mini kit (Qiagen, CA). Samples of total RNA (0.5 μg) were reverse transcribed following instructions in the Superscript III first strand synthesis kit (Invitrogen). The mouse VEGF mRNA level was measured by the AB 7500 Real-time PCR system (Applied

Author Manuscript Author Manuscript Author Manuscript Author Manuscript

Biosystems, CA). For each cell type or treatment, the amplification was conducted in a 10 μl of total volume containing 30 ng cDNA templates, 5 μl of 2× TaqMan Universal PCR Master Mix (Applied Biosystems, CA) and 0.5 μl of 20× mouse VEGF-c gene expression probe or GAPDH probe (assay IDs: Mm01202432_m1 for mouse VEGF and Hs99999909_m1 for GAPDH) (Applied Biosystems). The data are presented as the mean ratio of VEGF mRNA to GAPDH mRNA (±SD) obtained from triplicate samples.

Solute permeability measurement

The immortalized mouse brain endothelial cell line, bEnd3, was used due to their rapid monolayer formation and consistent blood-brain barrier characteristics over repeated passages [4, 22, 43]. The bEnd3 cells (66,000 per filter) were plated onto fibronectin (30μg/ml) coated transwell filter (pore diameter 0.4 μm, Corning, NY) and grown in DMEM/F-12 supplemented with 10% fetal bovine serum and 2 mM L-glutamine for approximately 4 days until confluent. After removal of culture medium and wash with PBS, 500 μL of 8 μM FITC-BSA in Ringer solution was added to the upper chamber of the transwell. Every 10 min for 2 hours, 50 μL of sample solution was collected from the bottom chamber of the transwell and then refilled with 50 μL of the BSA-Ringer solution. The fluorescence tracer concentration in the samples was determined by Bio-Tek Synergy HT plate reader (Winooski, VT), with excitation and emission wavelengths set to 485 nm and 535 nm, respectively. The permeability of bEnd3 monolayer to BSA, P^{BSA}, was calculated as follows:

$$P^{BSA}=\frac{\Delta C/\Delta t}{C_0}\cdot\frac{V}{A},$$

where $\Delta C/\Delta t$ is the increase in the fluorescence concentration in the bottom chamber during the time interval Δt, C_0 is the fluorescence concentration in the upper chamber (assumed to be constant during the experiment), V is the volume of the bottom chamber, and A is the surface area of the filter. In the case of VEGF treatment, 1 nM VEGF was present in both chambers, and also in the refilling solution; in the case of inhibiting VEGF receptor (KDR/Flk-1), the monolayers were pre-treated with 50 μM SU-1498 for 30 min before permeability measurement.

In vitro adhesion assay

Tumor cell adhesion to endothelial cells: mouse mammary epithelial normal (NMuMG) or tumor cells (WT and 1355T) were labeled using 1.0 μg/ ml Calcein AM in serum free medium for 20-30 min, trypsinized, washed with 1% BSA-Ringer solution and filtered using 40 μm cell strainer. After the fluorescence labeling, there were > 90% viable cells as determined by trypan blue exclusion. Then, each type of labeled cells (2×10^5/ml) in 1% BSA-Ringer solution were placed onto the confluent bEnd3 monolayer in 24-well plates and incubated for 15min, 1hr and 2hr. After gently washing away the non-adherent cells, the bEnd3 monolayer with adherent cells were imaged using a Nikon Eclipse TE2000-S microscope with 20× (NA=0.75) objective lens. Images were taken with a 12-bit CCD camera (Sensicam QE; Cooke, MI). 10 typical fields of 750 μm × 560 μm for each cell type were analyzed and the adhesion was determined as the number of adherent cells per 1 mm^2

Author Manuscript Author Manuscript Author Manuscript Author Manuscript

surface area of the bEnd3 monolayer. For integrin blocking tests, the tumor cells were pretreated with 20μg/ml of each corresponding antibody at 4 °C for one hour before adhesion assay; for the laminin-5 inhibition tests, the bEnd3 cell monolayers were pretreated with 20μg/ml of laminin-5 antibody for one hour before adhesion assay. In the case of VEGF treatment, 1 nM VEGF was present in both chambers, and also in the refilling solution; to inhibit endothelial VEGF receptor (KDR/Flk-1), the monolayers were pre-treated with 50 μM SU-1498 for 30 min. To examine the effect of endogenously secreted VEGF on the adhesion of WT and 1355T tumor cells to bEnd3 monolayers, a higher cell density of 6×10^5/ml was used.

Tumor cell adhesion to ECM proteins: 96-well plates were pre-coated with laminin-5 at increasing concentration series (from 0.08 to 10μg/ml) at 4 °C overnight. 0.01% BSA was used as a control. WT or 1355T cells with viability > 90% were plated at 50,000/well. After incubated at 37 °C for 1 hr, non-adherent cells were removed by a thorough wash with PBS. Adherent cells were fixed with 4% parafolmaldehyde and 20% methanol, stained with 0.5% crystal Violet in 20% methanol for 5 min. After gently washed with PBS, dye in cells was extracted with 0.1 M sodium citrate in 50% ethanol/water. Optical density of each well was captured at 595 nm using Bio-Tek Synergy HT plate reader.

Immunostaining

Staining of the endothelial junction proteins with and without adherent tumor cells: to determine the adhesion location of tumor cells to bEnd3, monolayers with adherent tumor cells were fixed with 1% parafolmaldehyde, permeabilized with 0.2% Triton 100-X, blocked with 10% BSA in 0.1% Triton 100-X/PBS solution for one hour, and incubated with primary rabbit polyclonal antibodies against ZO-1 or VE-cadherin in blocking solution (1:200) at 4°C overnight. After washed by PBS, the endothelial cell monolayers were incubated with Alexa Fluor 594 conjugated goat anti-rabbit IgG in blocking solution (1:500) for one hour. The cell nuclei were staining with DAPI in PBS (1:10,000). To determine VEGF effect on the junction proteins, after VEGF treatment, monolayers were fixed, permeabilized, blocked, and ZO-1 and VE-cadherin were stained in the same way as above.

Staining of the exposed laminin-5 at the luminal surface of bEnd3 monolayer: after confluent, monolayers were fixed with 4% paraformaldehyde, blocked with 10% BSA in PBS for 1 hr, primary mouse monoclonal antibody against laminin-5 (10 μg/ml) was added to the luminal surface of the monolayer and incubated at 4°C overnight. After washed by PBS, the endothelial cell monolayers were incubated with Alexa Fluor 488 conjugated goat anti-rabbit IgG in blocking solution (1:200) for 1 hr. Then the monolayers were permeabilized with 0.2% Triton 100-X, blocked with 10% BSA in 0.1% Triton 100-X/PBS solution for one hour, and stained with ZO-1 (as above). The cell nuclei were staining with DAPI in PBS (1:10,000).

Staining of the hemidesmosomal components: integrin β4 and BPAG-1 of tumor cells were co-stained to examine the formation of hemidesmosomes. WT and 1355T cells were placed on the plates pre-coated with 10μg/ml laminin-5, 10μg/ml fibronectin, or 0.01% BSA for 1 hr. After washing away the non-adherent cells, the adherent cells were fixed with 4% paraformaldehyde, permeabilized with 0.5% TritonX-100, blocked with 10% BSA and then

Author Manuscript Author Manuscript Author Manuscript Author Manuscript

double stained using 10 μg/ml of anti-human β4 (3E1) at 4°C overnight followed by an FITC-conjugated goat anti-mouse IgG (1:200), and 1 μg/ml of BPAG-1 polyclonal antibody at 4°C overnight followed by TR-conjugated donkey anti-goat IgG (1:200).

Fluorescence and confocal microscopy

Localizations of immunolabeled junction proteins ZO-1 and VE-cadherin in the bEnd3 monolayers, exposed laminin-5 at the luminal surface of bEnd3 monolayers, and the distribution of adherent tumor cells on cell monolayers and on ECM proteins were performed using a Nikon Eclipse TE2000-E microscope with objective lens 20× (NA=0.45) or 40× (NA=0.6). Images were taken with a Photometrics Cascade 650 CCD camera from Roper Scientific (Tucson, AZ). To observe the detailed distribution of laminin-5 and ZO-1 at a tri-cellular junction, we used a Zeiss LSM 510 laser scanning confocal microscope with objective lens 100× (NA=1.3). The lasers were set as blue Ex/Em: 405/470-500 nm, green Ex/Em: 488/505-530 nm, and red Ex/Em: 560/615 nm. The image stacks were analyzed with the NIH IMAGE J program. Stacks of 8 images were projected onto a single plane to obtain the final image, which has a thickness of 1.2 μm.

Analysis and statistics

All data were presented as mean ± SD or otherwise specified. Data were analyzed for statistical significance using a student t-test. χ^2 test was used to analyze the statistical significance of the distribution in the adhesion location of tumor cells. Significance was assumed for probability levels $p < 5\%$.

RESULTS

The β4 integrin promotes mammary tumor cell adhesion to microvascular endothelium

Since brain metastases develop in about 30% of breast cancer patients who relapse after adjuvant therapy [30], we decided to model *in vitro* the tumor adhesion to brain microvascular endothelium. Primary mammary tumor cells derived from MMTV-*Neu* mice were infected with a lentivirus encoding a shRNA designed to silence the expression of endogenous mouse β4 and then reconstituted with expression vectors encoding either wild-type or signaling-defective human β4, as previously described [16]. The latter mutant, which is truncated at amino acid 1355 and is therefore denoted as 1355T, lacks all major tyrosine phosphorylation sites and is unable to amplify oncogenic ErbB2 signaling [16]. Immunoblotting with an antibody reacting preferentially with the N-terminal portion of human β4 demonstrated that the Neu-β4-WT (here referred to as WT) cells and the Neu-β4-1355T (here referred to as 1355T) cells express similar levels of recombinant wild-type or mutant β4, respectively (first row in Fig. 1). As anticipated 1355T displayed faster electrophoretic mobility as compared to WT. Reprobing of the same samples with antibodies to the evolutionarily conserved C-terminal segment of β4 indicated that the Neu-transformed cells express β4 at significantly higher levels as compared to Normal Murine Mammary Gland (NMuMG) epithelial cells (second row in Fig. 1). As predicted, this antibody did not react with 1355T, because this mutant lacks the corresponding epitope, but it detected a small amount of endogenous wild-type β4 that had escaped silencing in 1355T cells. These results indicate that we have

Author Manuscript Author Manuscript Author Manuscript Author Manuscript

generated Neu-transformed cells that over-express similar levels of either wild-type or mutant β4.

To model the early phase of metastatic spread, we examined the ability of NMuMG, WT, and 1355T cells to adhere to a confluent monolayer of mouse brain microvascular endothelial cells (bEnd3) (Figs. 2a,b,c,d). Summary in Fig. 2d indicates that after 1 hr adhesion, the amount of adherent WT and 1355T cells were 1.7-fold and 1.8-fold, respectively, of that of adherent NMuMG cells ($n = 12$, $p < 0.01$). There was no significant difference in WT and 1355T adhesion at this time point ($n = 12$, $p = 0.59$). These results suggest that the β4 integrin promotes adhesion to an intact brain microvascular endothelium *in vitro*, but they exclude a role for its signaling domain in this process.

The β4 integrin is a transmembrane protein, which mediates adhesion, and in some cells assembly of hemidesmosomal junctions in response to binding to the basement membrane component laminin-5 [13]. To test if the β4 integrin mediates mammary tumor cell adhesion to brain microvascular endothelium, we performed antibody perturbation experiments. Since antibodies that effectively suppress the adhesive function of the β4 integrin by binding to the ectodomain of the β4 subunit are not commercially available, we used the GoH3 monoclonal antibody, which recognizes the ectodomain of the α6 subunit and blocks the adhesive function of both α6β1 and α6β4 (here referred to as the β4 integrin). We reasoned that using an antibody that also blocks α6β1 would have not confounded the interpretation of the experiments because the WT and 1355T cells do not express α6β1 (data not shown). Figure 2d shows that anti-α6 significantly reduced the WT and 1355T adhesion by the same level, by ~70% of their controls ($n = 6$, $p < 0.001$). Blocking laminin-5 impaired the WT adhesion by only 25%, and the 1355T adhesion by 15% ($n = 6$, $p < 0.04$), respectively, consistent with the hypothesis that the laminin-5 produced by endothelial cells is deposited in the basement membrane underneath the intact monolayer and is therefore inaccessible to the antibodies or the tumor cells unless exposed as a consequence of tumor action. In comparison, the normal NMuMG cell adhesion was not impaired by these antibodies ($n = 6$, $p > 0.26$). Results in Fig.2d suggest that the β4 integrin mediates initial adhesion of mammary tumor cell to bEnd3 endothelium by binding to an unidentified counter-receptor on endothelial cells.

Deletion of the β4 signaling domain does not reduce adhesion to laminin-5

Since laminin-5 is an ECM ligand of integrin β4, we performed the ligand-binding adhesion assay to examine the role of β4 signaling in tumor cell adhesion to laminin-5. 0.01% BSA/PBS was used as a control since laminin-5 was dissolved in 0.01% BSA/PBS solutions. Figure 3 shows that at concentrations higher than 0.16 μg/ml, both WT and 1355T cells adhere significantly more than the control (n=5, p<0.05). In contrast, for all the concentrations of laminin-5, there was no significant difference in WT and 1355T cell adhesion (n=5, p>0.07), indicating that deletion of the β4 signaling domain does not impair adhesion to laminin-5, but actually slightly increases this process at high concentrations of laminin-5.

Author Manuscript Author Manuscript Author Manuscript Author Manuscript

Deletion of the β4 signaling domain does not affect assembly of hemidesmosome-like adhesions on laminin-5

Since prior studies have indicated that phosphorylation of the β4 signaling domain causes a destabilization of hemidesmosomes [9, 23], we examined if the increased ability of 1355T cells to adhere to high concentrations of laminin-5 *in vitro* was due to increased formation of hemidesmosome-like adhesions by these cells. The major components of a hemidesmosome are a cytoplasmic protein bullous pemphigoid antigen-1 (BPAG-1), the transmembrane β4 integrin and laminin-5 at the ECM [36, 37, 42]. When β4 of the tumor cell binds to laminin-5, hemidesmosome is assembled, which is characterized by the co-localization of the cytoplasmic BPAG-1 and the transmembrane β4 of tumor cells. However, mammary tumor cells do not form large, easily detectable hemidesmosomes like keratinocytes *in vivo*, but small puncta. To study these puncta, we conducted quantitative co-localization experiments. Photomicrographs in Figs. 4a-f demonstrate the double immunostaining of hemidesmosome components, β4 (green) and BPAG-1 (red) after 1 hr WT and 1355T cell adhesion to 10 μg/ml of fibronectin (Figs. 4b1-3, e1-3) and laminin-5 (Figs.4c1-3, f1-3). A control group to 0.01% BSA is presented in (Figs. 4 a1-3, d1-3) since both fibronectin and laminin-5 were dissolved in 0.01% BSA. The amount of hemidesmosome-like adhesions was represented by the pixel numbers per μm^2 that was double-labeled for both β4 and BPAG-1 (orange color in Figs. 4a3-c3 and d3-f3). The same level of β4 and BPAG-1 expression of WT and 1355T (Figs. 4g, h) and the same level of co-localization of β4 and BPAG-1 (Fig. 4i) during their adhesion to laminin-5 suggest that β4 signaling does not interfere with the formation of hemidesmosome-like adhesions.

Integrin β4 signaling increases secretion of VEGF

Since VEGF increases tumor cell adhesion to the endothelium both *in vitro* and *in vivo* [21, 33], we used ELISA to monitor the ability of WT and 1355T cells to secrete VEGF over a 6 hrs time frame when plated alone (mono-culture) or in contact with the confluent bEnd3 monolayer (co-culture). Figure 5a demonstrates that under mono-culture conditions, significant VEGF secretion of WT and 1355T was observed after as short as 15 min incubation. After 15 min incubation, there was no difference in VEGF secretion between WT and 1355T ($p>0.2$) while after 1 hr or longer incubation, WT secreted 28-47% more VEGF than 1355T ($p<0.05$) under mono-culture and 8%-39% more under co-culture conditions (data not shown). In contrast, the VEGF secretion of bEnd3 monolayers was negligible even after 6 hr. Additionally, the VEGF secretion rate of WT cells increased as a function of time, it was 3.6 pg/10^5cells/hr during 0.25-1 hr, 6.9 and 13.4 pg/10^5cells/hr during 1-2 hr and 2-6 hr, respectively. The VEGF secretion rate of 1355T cells also increased, but only about 70%-85% of that of WT cells during the same time periods. A similar pattern of VEGF secretion was also observed during the co-culture with bEnd3 monolayers for both WT and 1355T cells (data not shown). These results suggest that β4 signaling controls secretion of VEGF by ErbB2-transformed mammary tumor cells.

VEGF increases mammary tumor cell adhesion to microvascular endothelium

As shown above, VEGF secretion increases with incubation time. The resulting enhanced VEGF level may affect WT and 1355T cell adhesion to bEnd3 monolayers. Figure 5b shows

Author Manuscript Author Manuscript Author Manuscript Author Manuscript

that WT and 1355T adhesion increased sharply during 0.25-1 hr at a rate of ~200 cells/mm^2/hr. Subsequently, the adhesion rates declined to 78 cells/mm^2/hr for WT and 20 cells/mm^2/hr for 1355T during the following hour. Differences in adhesion between WT and 1355T were evident beginning at 2 hr, and after 2 hr, the adhesion of WT cells to the bEnd3 monolayer continued to rise, though at a slower rate, while 1355T appeared to plateau. The correlation between increased secretion of VEGF and increased adhesion to microvascular endothelium observed over the 6 hrs time frame is consistent with the hypothesis that the WT cells adhere better because they secrete VEGF at an increased rate as compared to that of 1355T cells.

We next examined if addition of 1 nM exogenous VEGF normalizes the ability of 1355T cells to adhere to microvascular endothelium *in vitro*. We chose 1 nM VEGF because 1) it represents the secretion level of tumor cells observed after prolonged incubation; 2) it may reflect a local VEGF level in microvasculature near a solid tumor; and 3) it was shown to be an optimal dose that significantly increased tumor cell adhesion and endothelial permeability both *in vitro* and *in vivo* [21, 34]. Figure 6 shows WT and 1355T adhesion under control and under 1 nM VEGF treatment after 15 min, 1 hr and 2 hr incubation. After 15 min incubation, there was no difference in adhesion under control and under VEGF treatment ($p>0.3$) while there was a significant difference after 1 hr and 2 hr incubation under control and under VEGF treatment for both WT ($p<0.05$) and 1355T cells ($p<0.01$). The same as under control and VEGF treatment, there was a sharp increase in WT and 1355T adhesion during 0.25-1 hr and a continued increase from 1hr to 2hr. However, the increase rate under VEGF was 1.6-fold that of under control for WT adhesion during both 0.25-1 hr and 1-2 hr periods; it was 1.8-fold and 1.2-fold for 1355T adhesion, respectively. In 2 hrs, we did not observe any statistically significant difference in adhesion between WT and 1355T cells when the cells were plated in the presence of 1 nM VEGF or in the absence of VEGF at a tumor cell seeding density of 2×10^5/ml. These results indicate that addition of exogenous VEGF normalizes the ability of 1355T cells to adhere to microvascular endothelium *in vitro*, in agreement with the hypothesis that the WT cells adhere more than the 1355T cells in the absence of exogenous VEGF because they secret larger amounts of VEGF, which is above a threshold if the tumor cell seeding density is larger or incubation time is longer (Fig. 5b).

Pharmacological inhibition of ErbB2 suppresses expression of VEGF mRNA and reduces secretion of VEGF by mammary tumor cells

The WT and 1355T are HER2 (ErbB2)-overexpressing tumor cells. Previous studies have shown that the tyrosine kinase inhibitor Iressa inhibits not only EGFR but also ErbB2 activation and thereby suppresses the proliferation and invasion of ErbB2-overexpressing tumor cells [16, 25]. To examine the possibility that Iressa also inhibits WT and 1355T adhesion to bEnd3 endothelium by inhibiting VEGF secretion of WT and 1355T cells, we quantified the relative VEGF mRNA expression levels of WT and 1355T cells as well as their VEGF secretion under the treatment of Iressa. Figure 7a shows that after 1 hr Iressa treatment, the VEGF mRNA level of the WT decreased to 49% of its control level; it further decreased to 22% of the control after 6 hr and stayed the same after 12 hr treatment. The control VEGF mRNA level of the 1355T was only 54% of that of the WT; this level declined to 30% of the control after 1 hr Iressa treatment and stayed the same after 12 hr.

Author Manuscript Author Manuscript Author Manuscript Author Manuscript

Accordingly, Fig. 7b demonstrates corresponding changes in VEGF secretion by WT cells in response to Iressa treatment. After 1, 6 and 12 hr, Iressa decreased the VEGF secretion of WT cells to 50%, 67% and 55% of untreated controls. Iressa also decreased the secretion rate to 45%-75% of the control during these periods. In comparison, VEGF secretion of the 1355T was lower than that of the WT, about 39%, 55% and 39% of that of the WT at 1, 6 and 12 hr. Figure 7c shows that Iressa reduced VEGF secretion by 1355T cells to 36%, 49% and 33% of control levels at these times. The secretion rate was also reduced by Iressa to 36%-50% of the control from the beginning to 6 hr, and almost no secretion increase was observed from 6 to 12 hr under the Iressa treatment. Iressa effectively suppressed transcription of VEGF in both WT and 1355T cells, demonstrating that ErbB2 signaling is necessary for this process. Interestingly, however, Iressa did not completely suppress secretion of VEGF by the WT cells. Since prior studies have indicated that integrin β4 signaling controls translation of the VEGF mRNA [8], we infer that the β4 integrin cooperates with ErbB2 to promote transcription of VEGF and promote translation of the mRNA autonomously, i.e. without collaborating with ErbB2. Due to the decrease in the VEGF secretion, after 1 hr Iressa treatment, the adherent WT and 1355T cells to bEnd3 monolayers were only 70% and 60% of their controls, respectively (data not shown).

Pharmacological inhibition of the endothelial VEGF receptor coordinately diminishes the VEGF-induced increase in endothelial permeability and mammary tumor cell adhesion

As shown above, VEGF increases tumor cell adhesion to bEnd3 monolayers. To test whether VEGF exerts this effect by activating the endothelial VEGF receptor (VEGFR-2; KDR/Flk-1), we used SU-1498, a specific kinase inhibitor. We first measured the effects of VEGF and SU-1498 on bEnd3 monolayer permeability to BSA (MW ~67kD, radius~3.5nm). Figure 8a shows that VEGF significantly increased the bEnd3 monolayer permeability to BSA from a mean of 4.51 ± 0.75 to a mean of 6.19 ± 1.56 × 10^{-7} cm/s (n=6, p=0.045). While pretreatment with SU-1489 did not change the basal bEnd3 permeability, it did abolish the VEGF-enhanced permeability from 6.19 ± 1.56 to 4.53 ± 0.94 × 10^{-7} cm/s (n=6, p= 0.96 compared to the control). Then we examined the *in vitro* adhesion of WT and 1355T tumor cells to bEnd3 endothelium under the treatment of VEGF and SU-1498. Figure 8b shows that after 1 hr treatment, 1nM VEGF significantly enhanced the WT adhesion by 47% (n=6, p=0.0004) and the 1355T adhesion by 40% (n=6, p=0.045), respectively, compared to their controls. Pretreatment of bEnd3 monolayers with SU-1498 completely abolished this increased adhesion by VEGF (n=6, p>0.7 compared to the controls). These results indicate that VEGF promotes mammary tumor cell adhesion to microvascular endothelium by activating its cognate receptor tyrosine kinase on endothelial cells.

VEGF increases mammary tumor cell adhesion at or near endothelial cell junctions

To examine if VEGF affects initial adhesion to the apical surface of endothelial cells or the subsequent accumulation at cell junctions, which may correlate with their disruption and the eventual transmigration, we monitored the localization of attaching cells over time by using immunofluorescent staining. We grouped the locations of the adherent tumor cells into three categories: at the joint of two cells, at the joint of three (or more) cells and at the cell body. Figures 9a, b demonstrate the photomicrographs of WT and 1355T tumor cell adhesion to bEnd3 monolayers. Red lines are endothelial cell borders with ZO-1 labeling, blue spots are

Author Manuscript Author Manuscript Author Manuscript Author Manuscript

endothelial nuclei dyed with DAPI and green spots are tumor cells dyed with Calcein AM. Figures 9c-h show the distributions of adherent WT and 1355T to bEnd3 monolayers under control and under 1 nM VEGF treatment after 15 min, 1 hr and 2 hr incubation. For both WT and 1355T cells, the distributions of adhesion locations after 1 hr and 2 hr of VEGF treatment were significantly different from control ($p<0.005$, χ^2 test), while there was no difference under 15 min treatment ($p=0.47$ for WT and $p=0.13$ for 1355T, χ^2 test). For example, under control conditions, after 1 hr adhesion, there was a total of 47 ± 5 (mean ± SD, n = 3) adherent WT cells: 6 cells adhered to the bEnd3 cell bodies, 15 to the junctions of two bEnd3 cells and 26 to the junctions of three bEnd3 cells. Interestingly, after 1 hr VEGF treatment, the total adherent WT cells increased to 93 ± 11, of which, only 5 adhered to bEnd3 cell bodies, but 29 to the junctions of two bEnd3 cells and 59 to the junctions of three bEnd3 cells. The results indicate that VEGF treatment for 1 hr induced a slight decrease in the adherent WT cells to the bEnd3 cell bodies, but a significant increase in those to the bi-cellular (1.9-fold) and tri-cellular (2.3-fold) junctions. More interestingly, VEGF treatment for 2 hr significantly decreased WT adhesion to bEnd3 cell bodies (50%) relative to controls, and increased adhesion only to the tri-cellular junctions (1.4-fold). Similar trends were observed for 1355T adhesion. Our results clearly show that VEGF increases tumor cell adhesion to the bEnd3 monolayer by increasing its adhesion to the intercellular junctions instead of cell bodies.

VEGF disrupts the integrity of microvascular endothelial junctions

Since we had observed that activation of the VEGFR-2 on endothelial cells coordinately increases endothelial permeability and mammary tumor cell adhesion at or near endothelial intercellular junctions, we made the hypothesis that disruption of the integrity of the intercellular junctions would expose the underlying basement membrane leading to a further increase in adhesion. To test this hypothesis, we quantified the endothelial tight junction protein, Zonula occludens-1 (ZO-1), and adherens junction protein, vascular endothelial-cadherin (VE-cad) under control and under VEGF treatment. The relative amount of junction proteins was represented by the percentage of the cell border pixels having the intensity higher than the background intensity over the total pixel number of the cell border. To determine the background intensity, we first identified the cell border of bEnd3 cells by observing a sharp change in the fluorescence intensity of ZO-1/VE-cadherin staining (see Fig.10a). Then, we draw 6-7 cytoplasmic domains within the cell borders in a view field shown in Fig. 10a, and obtained the average intensity per pixel of staining in these cytoplasmic domains. This average intensity per pixel was determined as the background intensity. Figure 10a shows the photomicrographs of immunostaining of ZO-1 (upper panel) and VE-Cadherin (lower panel) of bEnd3 monolayers under control, and after 1 hr and 2 hr VEGF treatments, respectively. Figures 10b shows that ZO-1 was reduced from a mean of 0.99 ± 0.01 to a mean of 0.84 ± 0.03 after 1 hr VEGF treatment, and to a mean of 0.74±0.03 after 2 hr treatment ($n=6$, $p< 0.001$), while VE-Cadherin was reduced from a mean of 0.98 ± 0.01 to a mean of 0.63 ± 0.05 after 1 hr VEGF treatment, and to a mean of 0.47 ± 0.10 after 2 hr treatment ($n=6$, $p< 0.001$). The VEGF-induced disruption of junction assembly of bEnd3 endothelium is consistent with the increase in BSA permeability and tumor cell adhesion to the intercellular junctions.

Author Manuscript Author Manuscript Author Manuscript Author Manuscript

VEGF-mediated disruption of endothelial junctions renders the integrin β4 ligand laminin-5 accessible to mammary tumor cells

To test if the disruption of the integrity of bEnd3 intercellular junctions induced by VEGF leads to the exposure of laminin-5, the basement membrane ligand of the β4 integrin, we treated bEnd3 monolayers with or without VEGF and subjected them to immunofluorescent staining with antibodies to laminin-5. Upon confluent, bEnd3 monolayer shows significant amount of laminin-5 in its basement membrane as observed by confocal microscopy (data not shown) when immunostaining was carried out after first permeabilizing bEnd3 cells. To label the laminin-5 exposed at the luminal surface of the bEnd3 endothelium, we carried out the immunostaining without permeabilizing bEnd3 cells. The upper figure in Fig. 11a shows the laminin-5 (green) at the luminal surface of the bEnd3 monolayer, which was stained before permeabilizing the cells; the middle figure shows the junction protein ZO-1 (red) and cell nuclei (blue), which were stained after permeabilizing the cells; and the bottom figure shows the overlay of the upper and middle figures. The staining was carried out on cells not treated with VEGF (control shown in the left panel) and after 1 hr 1 nM VEGF treatment (shown in the right panel). Due to the resolution limitation of the optical microscope, it is almost impossible to see the exposed laminin-5 at the intercellular junctions under control conditions since the space at the intercellular junction was estimated to be 20-100 nm based on previous electron microscopy studies on HUVEC monolayers [5] and rat mesenteric microvessels [2]. In Fig.11b, a higher resolution confocal microscopic image shows the distribution of laminin-5 at a tri-cellular junction of the bEnd3 monolayer (region pointed by the arrow) after 1 hr VEGF treatment. Figure11c demonstrates that 15 min VEGF treatment did not significantly increase laminin-5 exposure ($p=0.06$), but 1 hr treatment significantly increased laminin-5 exposure to 7.0-fold of that under control ($p=0.0004$), 2 hr treatment further increased it to 2.5-fold of that after 1 hr treatment ($p=0.0001$). Increased laminin-5 exposure at the luminal surface of bEnd3 monolayer allows more binding between laminin-5 and β4 of WT and 1355T and thus increases their adhesion to the intercellular junctions of bEnd3 monolayers.

DISCUSSION

The β4 integrin promotes mammary tumorigenesis and metastasis by combining with ErbB2 and amplifying its signaling capacity. Deletion of the β4 signaling domain uncouples β4 from ErbB2, suppressing activation of STAT3 and c-Jun and thereby preventing the disruption of epithelial adhesion and hyperproliferation associated with ErbB2-mediated transformation, and reducing metastasis *in vivo* [16]. To examine the mechanism by which integrin β4 signaling promotes metastatic spread, we have modeled the first phase (e.g., adhesion) of this process *in vitro*. Our results indicate that the β4 integrin plays sequential, unexpected roles in this process. First, it contributes to the initial adhesion of mammary tumor cells to microvascular endothelium by binding to an unidentified counter-receptor on the apical surface of endothelial cells, as demonstrated by the observation that antibodies blocking the ligand binding pocket of β4 suppress this process by ~70%, whereas antibodies to laminin-5 only by ~25% or less. Second, the β4 integrin enhances the capacity of oncogenic ErbB2 to drive secretion of VEGF, which acts upon the endothelial cells to cause a partial disruption of both tight and adherens junctions. Our results are consistent with

Author Manuscript Author Manuscript Author Manuscript Author Manuscript

others for the VEGF effect on endothelial junction proteins and tumor metastasis [10, 12, 19, 40, 41]. Third, the ensuing exposure the underlying basement membrane enables β4 to mediate adhesion to this structure by binding to laminin-5 prior to the initiation of localized proteolysis that is necessary for transmigration into tissue stroma.

We have used the same expression vector, and thus promoter, to reconstitute the expression of either wild-type or mutant β4 in ErbB2-transformed mammary tumor cells. Immunoblotting experiments indicated that this approach has led to similar levels of expression of the mature form of either wild-type or mutant β4, suggesting that targeted deletion of the β4 signaling domain does not affect the biosynthesis or transport of β4 to the cell surface (Fig. 1). The β4 integrin promotes mammary tumor cell adhesion to brain microvascular endothelium (Fig. 2). Deletion of the β4 signaling domain does not reduce tumor cell adhesion to its ECM ligand laminin-5 (Fig. 3) nor affect the assembly of hemidesmosome-like puncta (Fig.4). Instead, β4 signaling enhances the ErbB2-depedent expression of VEGF by tumor cells to promote their adhesion to microvascular endothelium (Figs. 5, 6, 9) provided that the VEGF secretion reaches a threshold at which it is able to disrupt the junction proteins (Fig. 10) and expose enough laminin-5 (Fig. 11). Finally, we have shown that inhibition of ErbB2 on tumor cells or the VEGFR-2 on endothelial cells prevents mammary tumor cell adhesion to microvascular endothelium *in vitro* (Fig. 8). These results suggest the possibility that the therapeutic efficacy of existing ErbB2- and VEGFR2-targeted agents may be in part attributable to inhibition of metastatic spread and reseeding [28].

The observation that β4 mediates initial adhesion to microvascular endothelium, before VEGF-mediated disruption of endothelial junctions and exposure of the underlying basement membrane, suggests the existence of an unidentified counter-receptor on endothelial cells. A plausible candidate ligand is CLCA2, a calcium activated chloride channel protein. Studies by Abdel-Ghany et al.[1] showed that the colonization of the lungs by human breast cancer cells is correlated with cancer cell surface expression of α6β4 integrin and adhesion to CLCA2, which is expressed on the luminal surface of the endothelium lining pulmonary arterioles, capillaries and venules. β4 binding to CLCA2 may explain the observed ~20% adherent tumor cells at the bEnd3 cell bodies during the initial adhesion.

Another interesting observation is that there is a preferential location for tumor cell adhesion to bEnd3 monolayers especially after VEGF treatment. Since a significant portion of the bEnd3 endothelial monolayer is occupied by the junctions of endothelial cells, we performed a calculation to determine the probability of the tumor cells adhering to the junctions for a random distribution of adhesion. Using the same method described in He et al. (2000) [17], we first measured the length of the endothelial junctions per unit area of bEnd3 endothelial monolayers by tracing the ZO-1 labeling at the endothelial cell borders from 10 images similar to Fig. 10a. The averaged value is 83.4±4.5 mm/mm^2. If we expand this junction length to a 6.3 μm wide band, which is half of the contact length (diameter) of a tumor cell, the calculated band area is ~53% (6.3μm × 83.4 mm/mm^2) of the total area of the bEnd3 monolayer without the exclusion of the overlap at the tricellular junctions. This calculation indicates that the maximum probability of tumor cells adhering to the junctions by a random process is about 53%. Any value greater than 53% represents a preferential adhesion to the

Author Manuscript Author Manuscript Author Manuscript Author Manuscript

junctions. Even for the initial adhesion, ~80% tumor cells adhered to the intercellular junctions. VEGF enhanced tumor cell adhesion to the intercellular junctions, reaching ~95% after 1 hr treatment (Fig. 9c-h). One explanation for this preferential adhesion is that the overexpressed β4 at tumor cells prefers to bind to its ECM ligand, laminin-5, which is exposed at the junctions. Our results (Figs.10, 11) show that VEGF disrupted integrity of the intercellular junctions to enable more laminin-5 available for binding and thus increase the adhesion at junctions. Another explanation is that there are other cell adhesion molecules at the intercellular junctions, which can bind to β4 or other integrins at tumor cells. Burns et al. [5] found that there are P-selectins disseminating on the borders of cultured endothelial cells, which are responsible for the initial arrest of leukocytes. It is possible that P-selectin is involved in tumor cell adhesion. Another candidate is junctional adhesion molecule (JAM), which distributes at intercellular junctions of endothelial cells and was found to modulate monocyte transmigration [24]. JAM-1, a ligand of the β2 integrin of leukocytes, was involved in transendothelial migration of leukocytes [29]. Santoso et al. [31] reported that the homophilic binding of JAM-C mediates the adhesion of a lung carcinoma cell to endothelial cells (HUVEC). Since JAMs co-distribute with tight junction components at the apical region of the intercellular cleft [24], they have a location advantage for tumor adhesion if they can bind to receptors at the tumor cells. Future studies will be conducted to examine the role of JAMs in tumor adhesion.

Burns et al [6] found that neutrophils preferentially migrate across HUVEC monolayers at tricellular corners rather than through the bicellular junctions. In the current study, we found similar preferential adhesion of tumor cells to the tricellular junctions, especially after VEGF treatment. Compared to the control for the same adhesion time, 2 hr VEGF treatment induced a 1.4-fold enhancement in the tumor cell adhesion to the tricellular junction of bEnd3 monolayers, no change in the adhesion to the bicellular junctions and 50% decrease in that to the cell bodies (Figs. 9g, h). Preferential adhesion to the tricellular junctions suggests a potential path for tumor cell transmigration (extravasation), which will be investigated in our future research.

In our short term adhesion, due to the resolution limitation of the optical microscopy, we could not see the direct contact of tumor cells with the underlying basement membrane. Using electron microscopy, Weis et al. [41] found that the VEGF-expressing murine colon carcinoma cell extended its processes between endothelial junctions to directly contact the underlying basement membrane of the lung microvascular endothelium after hours of intravenous injection. Using real-time multiphoton laser scanning microscopy, Kienast et el. [20] revealed the single steps of mouse brain metastasis formation by human lung carcinoma and melanoma cells. They found that in minutes after internal carotid artery injection, ~10% of the injected tumor cells were stuck in vessel branches with the vessel diameter the same as that of the tumor cell. However, the extravasating cells could only been detected after day 1. Therefore, to investigate tumor cell adhesion to the underlying basement membrane and further transmigration across the brain microvascular endothelium, we must wait for much longer time than 6 hrs in the future study.

In conclusion, our results suggest that the β4 integrin plays sequential, adhesive and signaling roles during the initial phase of the metastatic spread of ErbB2-transformed

Author Manuscript Author Manuscript Author Manuscript Author Manuscript

mammary tumor cells. Our observation that β4 enables ErbB2 to upregulate expression of VEGF, which in turn promotes local disruption of endothelial cell junctions, identifies a novel mechanism potentially amenable to therapeutic inhibition.

ACKNOWLEDGEMENT

This work was supported by NIH grants P20 CA118861, U54 CA137788, SC1 CA153325, R37 CA058976, R01 CA129023, as well as P30 CA08748. Mr. Jie Fan was partially supported by a scholarship from the China Scholarship Council. We thank Dr. Robert Majeska for his kind helps in language editing.

REFFERENCES

1. Abdel-Ghany M, Cheng HC, Elble RC, Pauli BU. Focal adhesion kinase activated by beta(4) integrin ligation to mCLCA1 mediates early metastatic growth. J Biol Chem. 2002; 277:34391–34400. [PubMed: 12110680]
2. Adamson RH, Lenz JF, Zhang X, Adamson GN, Weinbaum S, Curry FE. Oncotic pressures opposing filtration across non-fenestrated rat microvessels. J Physiol. 2004; 557:889–907. [PubMed: 15073281]
3. Astolfi A, Landuzzi L, Nicoletti G, De Giovanni C, Croci S, Palladini A, Ferrini S, Iezzi M, Musiani P, Cavallo F, Forni G, Nanni P, Lollini PL. Gene expression analysis of immune-mediated arrest of tumorigenesis in a transgenic mouse model of HER-2/neu-positive basal-like mammary carcinoma. Am J Pathol. 2005; 166:1205–1216. [PubMed: 15793299]
4. Brown RC, Morris AP, O'Neil RG. Tight junction protein expression and barrier properties of immortalized mouse brain microvessel endothelial cells. Brain Res. 2007; 1130:17–30. [PubMed: 17169347]
5. Burns AR, Bowden RA, Abe Y, Walker DC, Simon SI, Entman ML, Smith CW. P-selectin mediates neutrophil adhesion to endothelial cell borders. J Leukoc Biol. 1999; 65:299–306. [PubMed: 10080531]
6. Burns AR, Walker DC, Brown ES, Thurmon LT, Bowden RA, Keese CR, Simon SI, Entman ML, Smith CW. Neutrophil transendothelial migration is independent of tight junctions and occurs preferentially at tricellular corners. J Immunol. 1997; 159:2893–2903. [PubMed: 9300713]
7. Chambers AF, Groom AC, MacDonald IC. Dissemination and growth of cancer cells in metastatic sites. Nat Rev Cancer. 2002; 2:563–572. [PubMed: 12154349]
8. Chung J, Bachelder RE, Lipscomb EA, Shaw LM, Mercurio AM. Integrin (alpha 6 beta 4) regulation of eIF-4E activity and VEGF translation: a survival mechanism for carcinoma cells. J Cell Biol. 2002; 158:165–174. [PubMed: 12105188]
9. Dans M, Gagnoux-Palacios L, Blaikie P, Klein S, Mariotti A, Giancotti FG. Tyrosine phosphorylation of the beta 4 integrin cytoplasmic domain mediates Shc signaling to extracellular signal-regulated kinase and antagonizes formation of hemidesmosomes. J Biol Chem. 2001; 276:1494–1502. [PubMed: 11044453]
10. Fischer S, Wobben M, Marti HH, Renz D, Schaper W. Hypoxia-induced hyperpermeability in brain microvessel endothelial cells involves VEGF-mediated changes in the expression of zonula occludens-1. Microvasc Res. 2002; 63:70–80. [PubMed: 11749074]
11. Fu BM, Shen S. Acute VEGF effect on solute permeability of mammalian microvessels in vivo. Microvasc Res. 2004; 68:51–62. [PubMed: 15219420]
12. Gavard J, Gutkind JS. VEGF controls endothelial-cell permeability by promoting the beta-arrestin-dependent endocytosis of VE-cadherin. Nat Cell Biol. 2006; 8:1223–1234. [PubMed: 17060906]
13. Giancotti FG. Targeting integrin beta4 for cancer and anti-angiogenic therapy. Trends Pharmacol Sci. 2007; 28:506–511. [PubMed: 17822782]
14. Giancotti FG, Ruoslahti E. Integrin signaling. Science. 1999; 285:1028–1032. [PubMed: 10446041]
15. Guo W, Giancotti FG. Integrin signalling during tumour progression. Nat Rev Mol Cell Biol. 2004; 5:816–826. [PubMed: 15459662]

Author Manuscript Author Manuscript Author Manuscript Author Manuscript

16. Guo W, Pylayeva Y, Pepe A, Yoshioka T, Muller WJ, Inghirami G, Giancotti FG. Beta 4 integrin amplifies ErbB2 signaling to promote mammary tumorigenesis. Cell. 2006; 126:489–502. [PubMed: 16901783]
17. He P, Wang J, Zeng M. Leukocyte adhesion and microvessel permeability. Am J Physiol Heart Circ Physiol. 2000; 278:H1686–1694. [PubMed: 10775150]
18. Hood JD, Cheresh DA. Role of integrins in cell invasion and migration. Nat Rev Cancer. 2002; 2:91–100. [PubMed: 12635172]
19. Khanna P, Yunkunis T, Muddana HS, Peng HH, August A, Dong C. p38 MAP kinase is necessary for melanoma-mediated regulation of VE-cadherin disassembly. Am J Physiol Cell Physiol. 2010; 298:C1140–1150. [PubMed: 20181932]
20. Kienast Y, von Baumgarten L, Fuhrmann M, Klinkert WE, Goldbrunner R, Herms J, Winkler F. Real-time imaging reveals the single steps of brain metastasis formation. Nat Med. 2010; 16:116–122. [PubMed: 20023634]
21. Lee TH, Avraham HK, Jiang S, Avraham S. Vascular endothelial growth factor modulates the transendothelial migration of MDA-MB-231 breast cancer cells through regulation of brain microvascular endothelial cell permeability. J Biol Chem. 2003; 278:5277–5284. [PubMed: 12446667]
22. Li G, Simon MJ, Cancel LM, Shi ZD, Ji X, Tarbell JM, Morrison B 3rd, Fu BM. Permeability of endothelial and astrocyte cocultures: in vitro blood-brain barrier models for drug delivery studies. Ann Biomed Eng. 2010; 38:2499–2511. [PubMed: 20361260]
23. Litjens SH, de Pereda JM, Sonnenberg A. Current insights into the formation and breakdown of hemidesmosomes. Trends Cell Biol. 2006; 16:376–383. [PubMed: 16757171]
24. Martin-Padura I, Lostaglio S, Schneemann M, Williams L, Romano M, Fruscella P, Panzeri C, Stoppacciaro A, Ruco L, Villa A, Simmons D, Dejana E. Junctional adhesion molecule, a novel member of the immunoglobulin superfamily that distributes at intercellular junctions and modulates monocyte transmigration. J Cell Biol. 1998; 142:117–127. [PubMed: 9660867]
25. Moasser MM, Basso A, Averbuch SD, Rosen N. The tyrosine kinase inhibitor ZD1839 (“Iressa”) inhibits HER2-driven signaling and suppresses the growth of HER2-overexpressing tumor cells. Cancer Res. 2001; 61:7184–7188. [PubMed: 11585753]
26. Muller WJ, Sinn E, Pattengale PK, Wallace R, Leder P. Single-step induction of mammary adenocarcinoma in transgenic mice bearing the activated c-neu oncogene. Cell. 1988; 54:105–115. [PubMed: 2898299]
27. Nikolopoulos SN, Blaikie P, Yoshioka T, Guo W, Giancotti FG. Integrin beta4 signaling promotes tumor angiogenesis. Cancer Cell. 2004; 6:471–483. [PubMed: 15542431]
28. Norton L, Massague J. Is cancer a disease of self-seeding? Nat Med. 2006; 12:875–878. [PubMed: 16892025]
29. Ostermann G, Weber KS, Zernecke A, Schröder A, Weber C. JAM-1 is a ligand of the beta(2) integrin LFA-1 involved in transendothelial migration of leukocytes. Nat Immunol. 2002; 3:151–8. [PubMed: 11812992]
30. Palmieri D, Smith QR, Lockman PR, Bronder J, Gril B, Chambers AF, Weil RJ, Steeg PS. Brain metastases of breast cancer. Breast Dis. 2006; 26:139–147. [PubMed: 17473372]
31. Santoso S, Orlova VV, Song K, Sachs UJ, Andrei-Selmer CL, Chavakis T. The homophilic binding of junctional adhesion molecule-C mediates tumor cell-endothelial cell interactions. J Biol Chem. 2005; 280:36326–36333. [PubMed: 16118203]
32. Senger DR, Perruzzi CA, Feder J, Dvorak HF. A highly conserved vascular permeability factor secreted by a variety of human and rodent tumor cell lines. Cancer Res. 1986; 46:5629–5632. [PubMed: 3756910]
33. Serini G, Trusolino L, Saggiorato E, Cremona O, De Rossi M, Angeli A, Orlandi F, Marchisio PC. Changes in integrin and E-cadherin expression in neoplastic versus normal thyroid tissue. J Natl Cancer Inst. 1996; 88:442–449. [PubMed: 8618236]
34. Shen S, Fan J, Cai B, Lv Y, Zeng M, Hao Y, Giancotti FG, Fu BM. Vascular endothelial growth factor enhances cancer cell adhesion to microvascular endothelium in vivo. Exp Physiol. 2010; 95:369–379. [PubMed: 19880535]

Author Manuscript Author Manuscript Author Manuscript Author Manuscript

35. Slamon DJ, Clark GM, Wong SG, Levin WJ, Ullrich A, McGuire WL. Human breast cancer: correlation of relapse and survival with amplification of the HER-2/neu oncogene. Science. 1987; 235:177–182. [PubMed: 3798106]

36. Spinardi L, Einheber S, Cullen T, Milner TA, Giancotti FG. A recombinant tail-less integrin beta 4 subunit disrupts hemidesmosomes, but does not suppress alpha 6 beta 4-mediated cell adhesion to laminins. J Cell Biol. 1995; 129:473–487. [PubMed: 7721947]

37. Spinardi L, Ren YL, Sanders R, Giancotti FG. The beta 4 subunit cytoplasmic domain mediates the interaction of alpha 6 beta 4 integrin with the cytoskeleton of hemidesmosomes. Mol Biol Cell. 1993; 4:871–884. [PubMed: 8257791]

38. Steeg PS, Theodorescu D. Metastasis: a therapeutic target for cancer. Nat Clin Pract Oncol. 2008; 5:206–219. [PubMed: 18253104]

39. Trusolino L, Bertotti A, Comoglio PM. A signaling adapter function for alpha6beta4 integrin in the control of HGF-dependent invasive growth. Cell. 2001; 107:643–654. [PubMed: 11733063]

40. Wang W, Dentler WL, Borchardt RT. VEGF increases BMEC monolayer permeability by affecting occludin expression and tight junction assembly. Am J Physiol Heart Circ Physiol. 2001; 280:H434–440. [PubMed: 11123261]

41. Weis S, Cui J, Barnes L, Cheresh D. Endothelial barrier disruption by VEGF-mediated Src activity potentiates tumor cell extravasation and metastasis. J Cell Biol. 2004; 167:223–229. [PubMed: 15504909]

42. Xia Y, Gil SG, Carter WG. Anchorage mediated by integrin alpha6beta4 to laminin 5 (epiligrin) regulates tyrosine phosphorylation of a membrane-associated 80-kD protein. J Cell Biol. 1996; 132:727–740. [PubMed: 8647901]

43. Yuan W, Li G, Gil ES, Lowe TL, Fu BM. Effect of surface charge of immortalized mouse cerebral endothelial cell monolayer on transport of charged solutes. Ann Biomed Eng. 2010; 38:1463–1472. [PubMed: 20087768]

Author Manuscript Author Manuscript Author Manuscript Author Manuscript

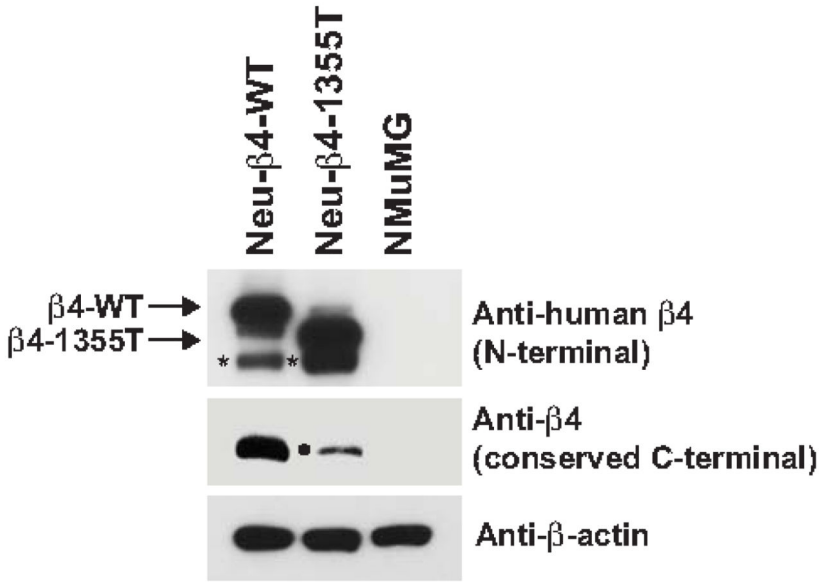

Fig.1.

β4 integrin expression of the ErbB2-transformed mouse mammary tumor cells (Neu-β4-WT and Neu-β4-1355T) expressing either wild type β4 (β4-WT) or β4 signaling defect (β4-1355T), and a normal murine mammary gland (NMuMG) epithelial cell line. Cells were lysed and subjected to immunoblotting with anti-β4 and anti-β-actin. * proteolytic fragment of recombinant human β4. • residual endogenous mouse β4.

Author Manuscript Author Manuscript Author Manuscript Author Manuscript

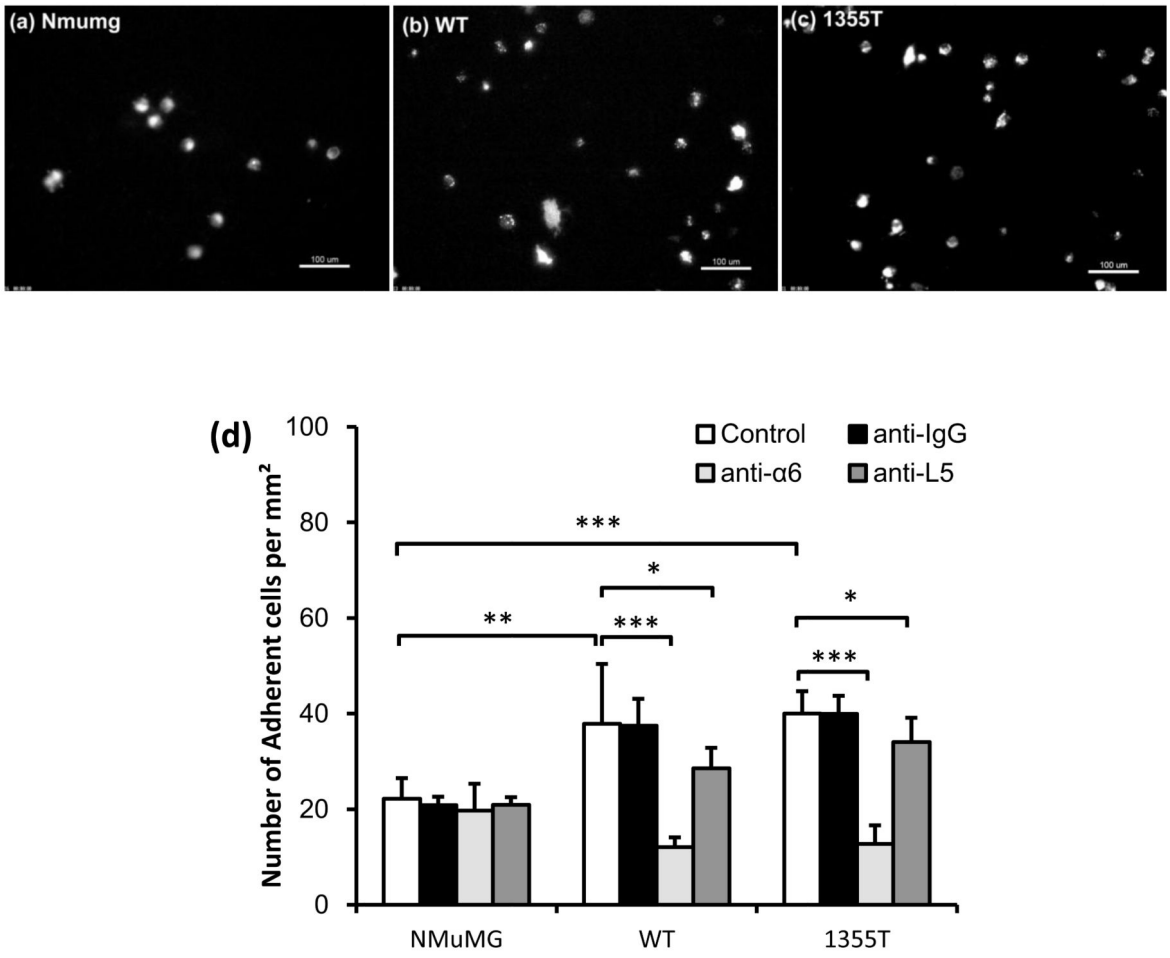

Fig.2.

(a) NMuMG, **(b)** WT and **(c)** 1355T cell adhesion to bEnd3 cell monolayers. Adhesion was measured 1 hr after seeding under control conditions. The bright spots indicate the adherent fluorescently-labeled cells observed after washing away unattached cells. **(d)** Comparison of adhesion density (number of adherent cells per unit area of the bEnd3 monolayer) of NMuMG, WT and 1355T cells under control (n=12) and under anti-integrin α6 (n=6) and anti-laminin-5 (n=6) treatment. Anti-mouse IgG was used as a sham control. Cell seeding density of NMuMG, WT and 1355T cells was 2×10^5/ml. The deposit time for both control and treatments was 1 hr. Ten typical fields of 750 μm × 560 μm per run for each cell type were analyzed. *p<0.05, **p<0.01, ***p<0.001.

Author Manuscript Author Manuscript Author Manuscript Author Manuscript

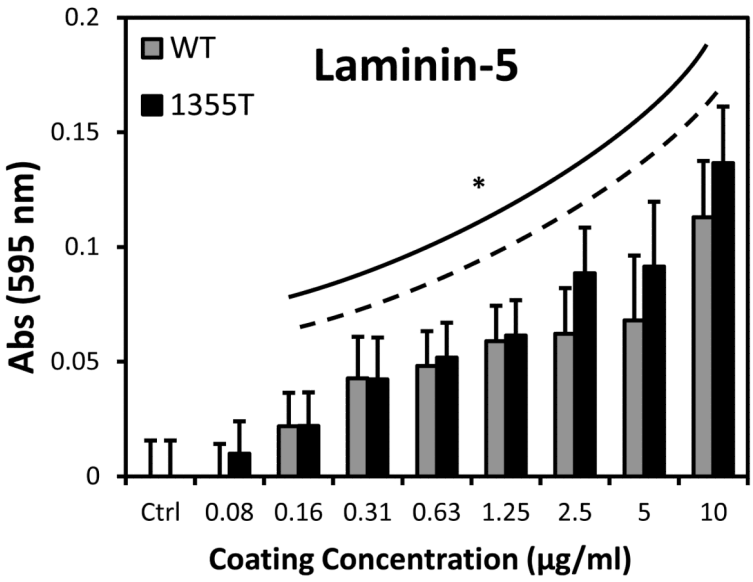

Fig.3.

WT and 1355T cell adhesion to laminin-5. WT and 1355T cells of the same passage were placed in the 96-well plate pre-coated with laminin-5 at the graded concentrations. After incubation for 1 hr and removal of unattached cells, the adherent cells in each well were determined by the absorbance as described in the main text. The solid line indicates that there is a significant difference in WT adhesion to ECM proteins compared to the control group (0.01% BSA); the dashed line shows adhesion of 1355T. n=5 for each concentration. *$p<0.05$ compared to the control (n=8).

Author Manuscript Author Manuscript Author Manuscript Author Manuscript

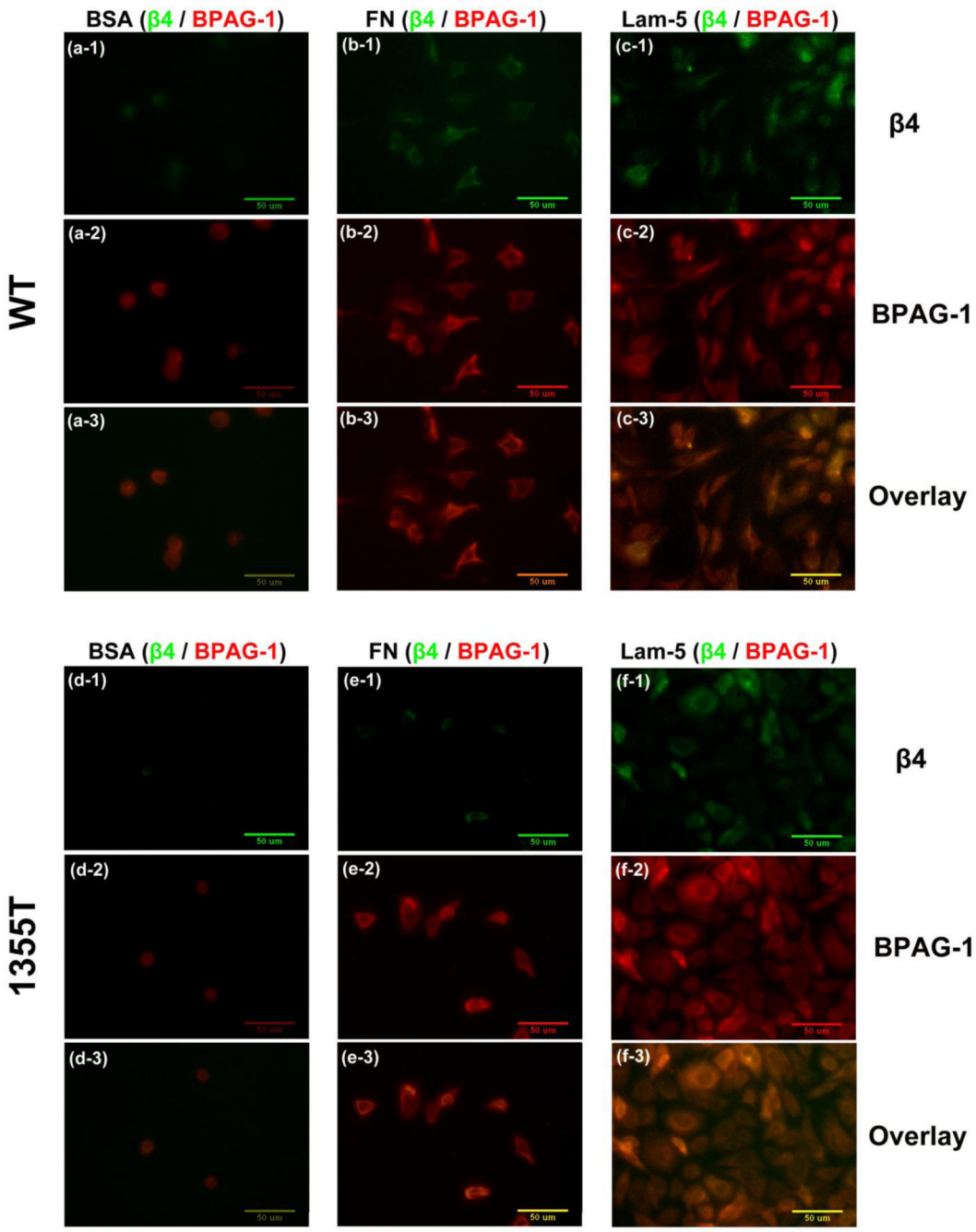

Author Manuscript Author Manuscript Author Manuscript Author Manuscript

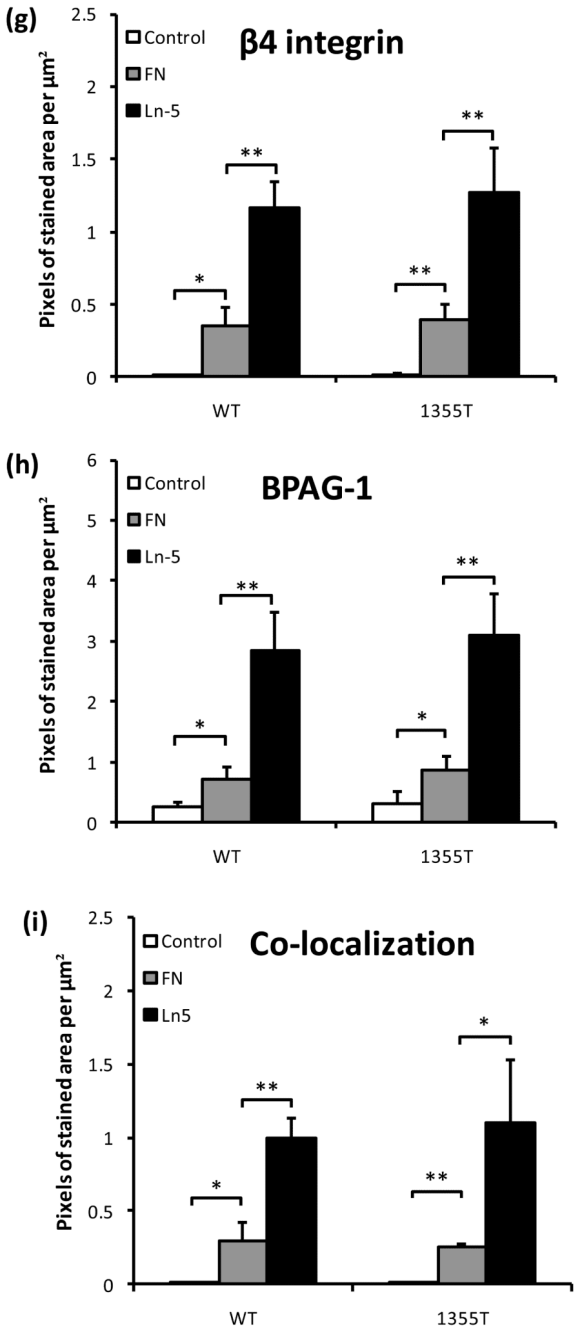

Fig.4.

Images of fluorescently-labeled hemidesmosomal marker proteins, β4 integrin (green) and BPAG-1 (red), and the overlay of β4 and BPAG-1 (orange). WT (upper panel) and 1355T (lower panel) tumor cell were allowed to adhere to 10 μg/ml of fibronectin **(b, e)** and laminin-5 **(c, f)**. Control group adhesion to 0.01% BSA is shown in panels **a** and **d**. The amount of β4 integrin and BPAG-1 in tumor cells was quantified based on the pixel numbers of the green labeled area or the red labeled area per μm^2, respectively, and related to the total image area, in **(g)** and **(h)**. The amounts of hemidesmosomes were quantified by the co-

localization of β4 integrin and BPAG-1, the orange labeled area, in **(i)**. n=3, *p<0.05, **p<0.01.

Author Manuscript Author Manuscript Author Manuscript Author Manuscript

Author Manuscript Author Manuscript Author Manuscript Author Manuscript

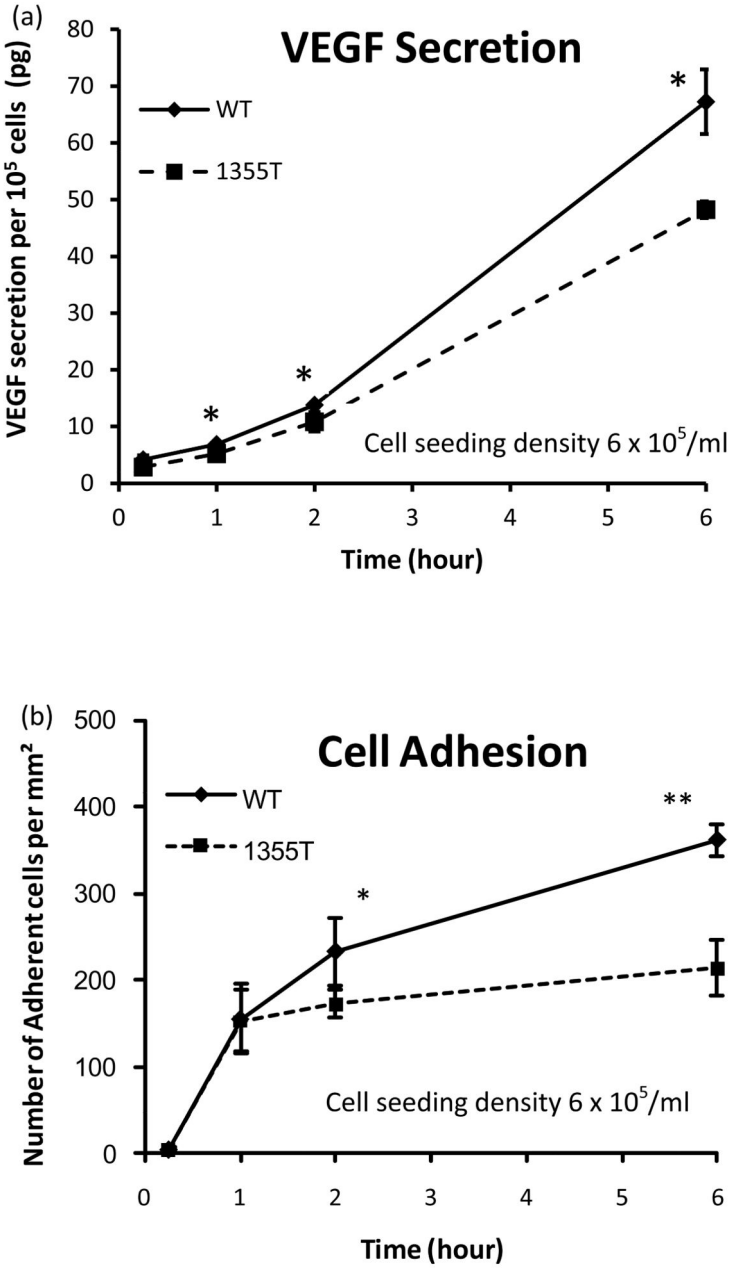

Fig.5.

(a) Comparison of temporal VEGF expression profiles of WT and 1355T tumor cells. **(b)** WT and 1355T tumor cell adhesion to bEnd3 monolayer was assessed at the indicated times. The tumor cell seeding density was 6×10^5/ml. n=3, * $p<0.05$, **$p<0.01$.

Author Manuscript Author Manuscript Author Manuscript Author Manuscript

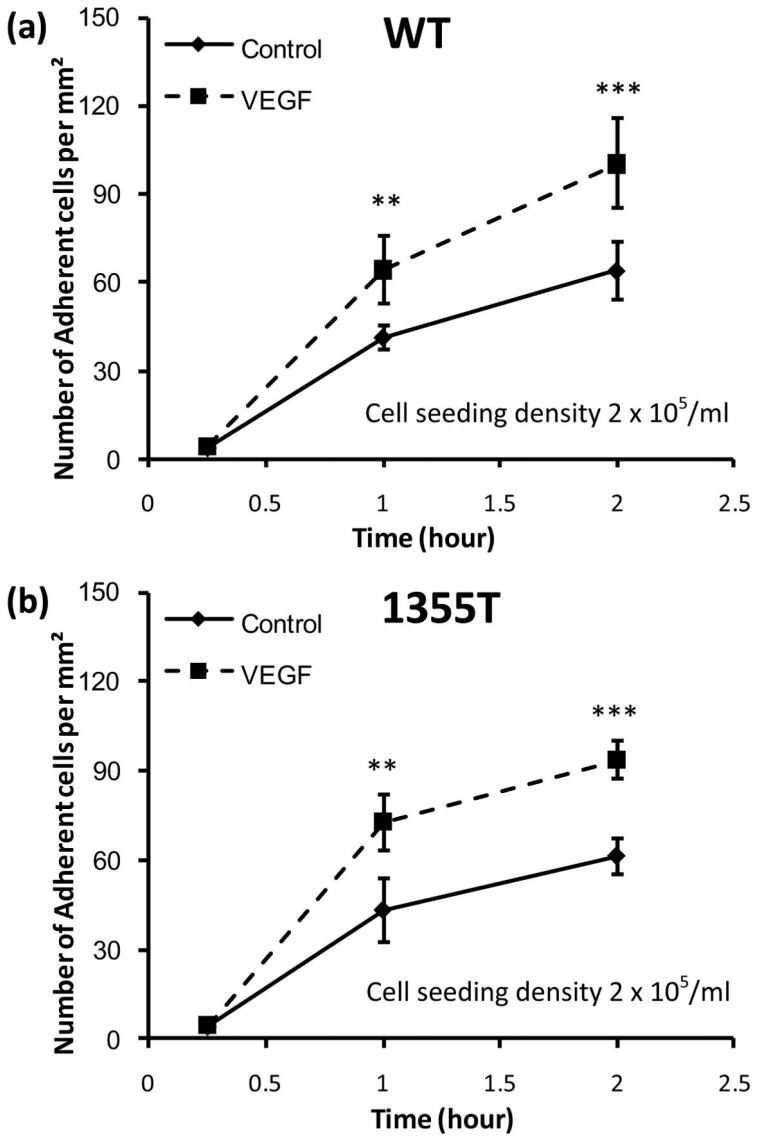

Fig.6.

Tumor cell **(a)** WT and **(b)** 1355T adhesion as a function of time under control and 1 nM VEGF treatment. The tumor cell seeding density was 2×10^5/ml. n=4, *p<0.05, **p<0.01, ***p<0.001.

Author Manuscript Author Manuscript Author Manuscript Author Manuscript

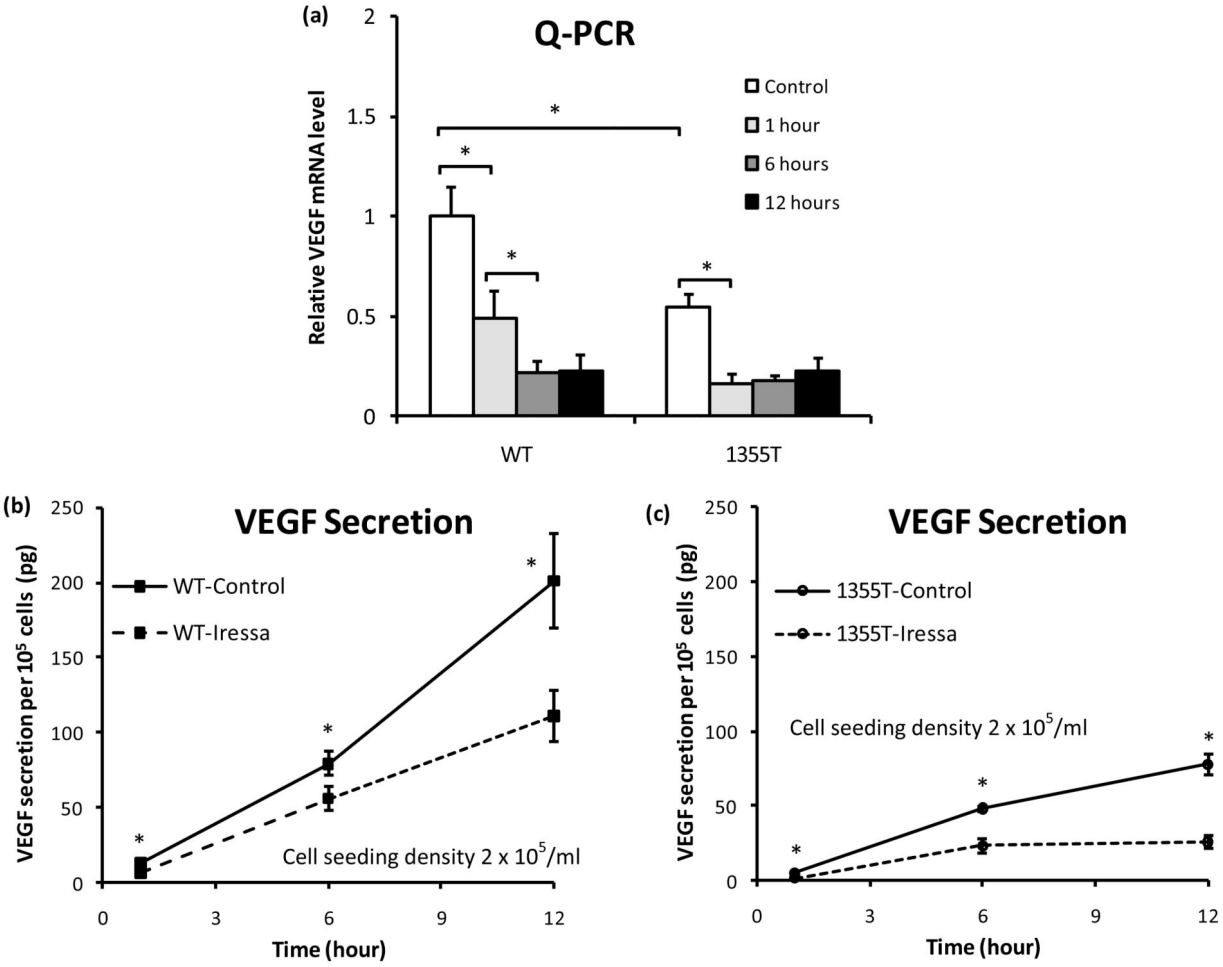

Fig. 7.

(a) VEGF mRNA levels in WT and 1355T cells. Total RNA was isolated from cells under control and Iressa (10 μM) treatment for the indicated times, and VEGF RNA was quantified by Q-PCR. The data are presented as the ratio of VEGF to GAPDH mRNA (mean±SD) obtained from triplicate samples. The VEGF secretion was quantified by ELISA for **(b)** WT and **(c)** 1355T cells under control and under the Iressa treatment at the indicated times. Results are the mean±SD of triplicate samples. Similar results were obtained from two independent experiments. *$p<0.05$ compared with the control.

Author Manuscript Author Manuscript Author Manuscript Author Manuscript

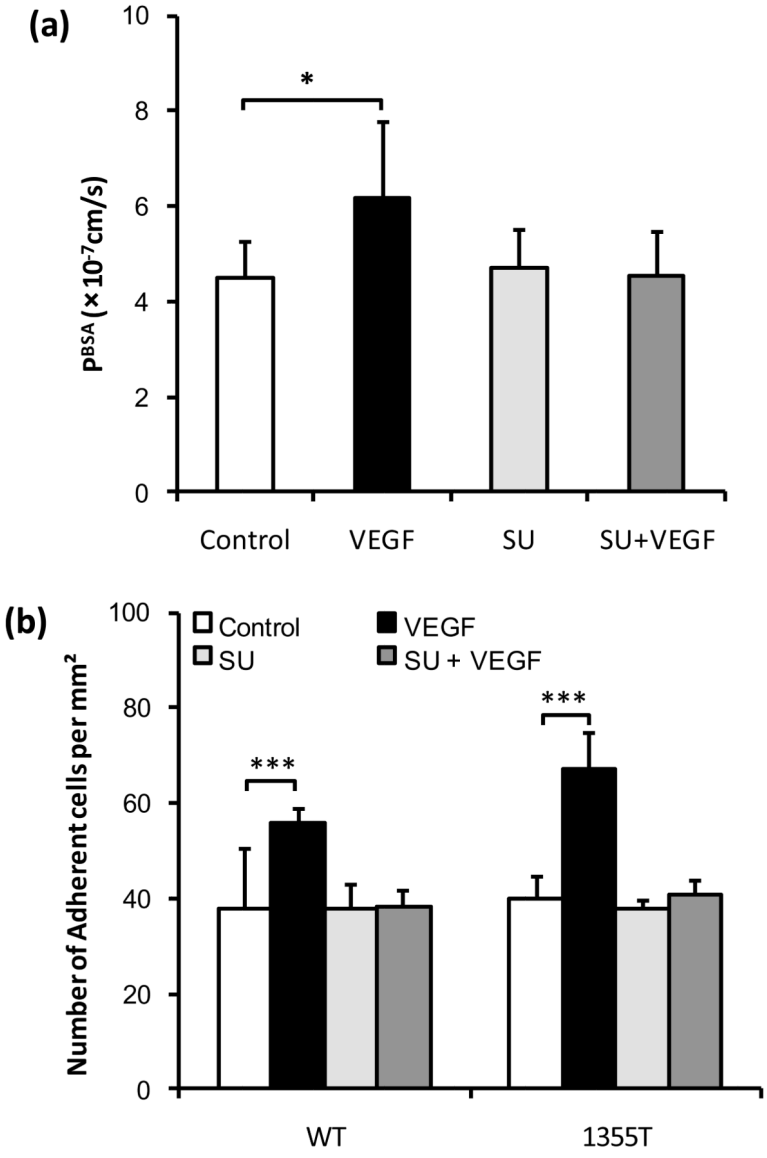

Fig.8.

Effects of VEGF and the endothelial VEGF receptor (KDR/Flk-1) inhibitor SU-1498 on **(a)** Permeability of the bEnd3 monolayer to albumin (n=6) and **(b)** WT and 1355T tumor cell adhesion. Permeability and adhesion were measured after 1 hr control and VEGF treatment. For inhibition by SU-1498, the bEnd3 monolayer was pretreated with SU-1498 for 30 min. In **(b)**, ten typical fields of 750 μm × 560 μm per run for each cell type in n=6 runs were analyzed. *p=0.045, ***p<0.001.

Author Manuscript Author Manuscript Author Manuscript Author Manuscript

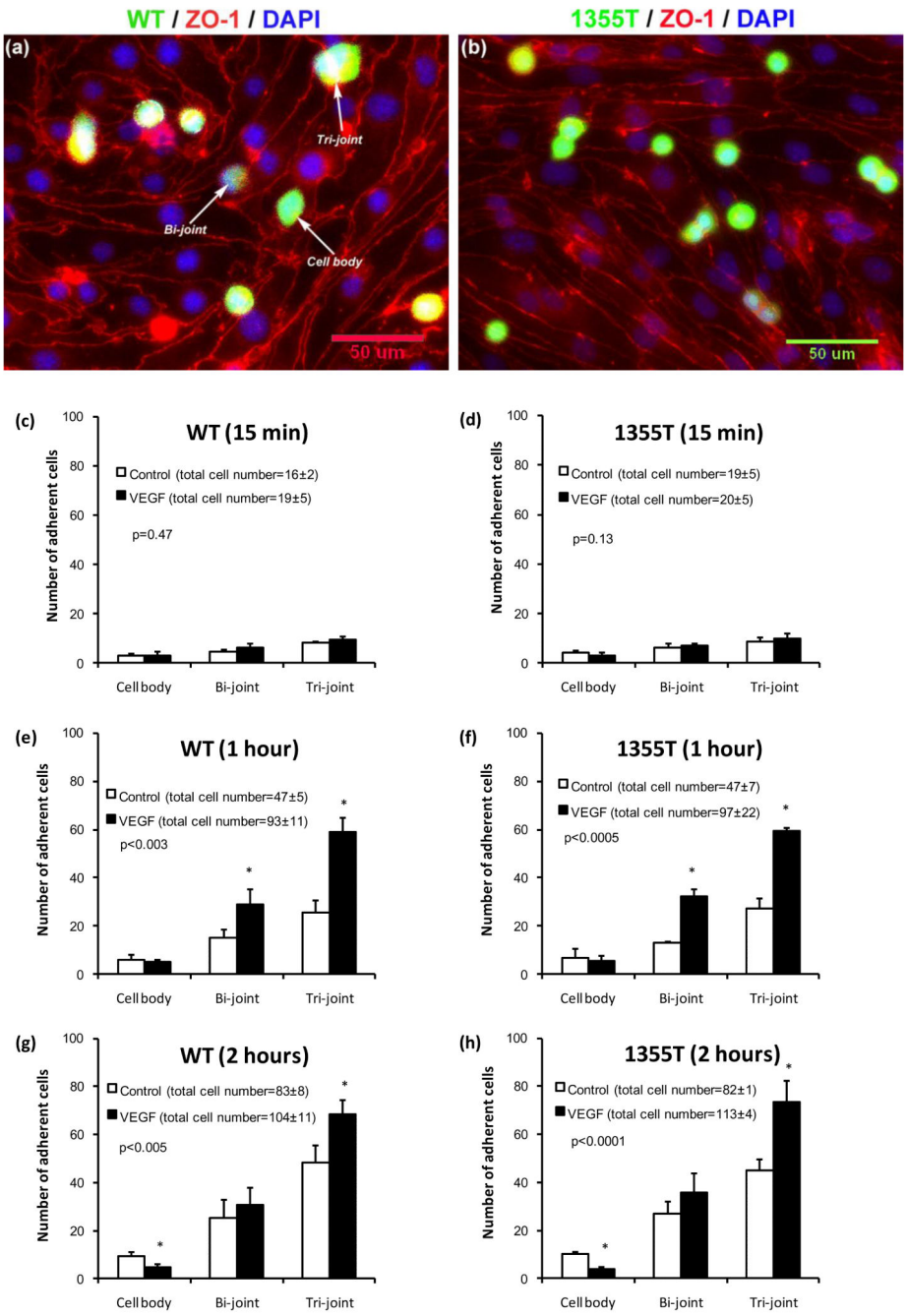

Fig.9.

Histogram of adhesion locations of tumor cells to bEnd3 monolayers under control and VEGF treatment. Typical fluorescent images for **(a)** WT and **(b)** 1355T cell adhesion after 1 hr VEGF treatment. Green spots are the tumor cells, red lines are tight junction proteins ZO-1 of the bEnd3 monolayer, and blue spots are bEnd3 endothelial cell nuclei. Summary of adhesion locations for WT **(c, e, g)** and 1355T **(d, f, h)** cells under control and 1 nM VEGF treatments for 15 min, 1 hr and 2 hr, respectively. Cell body represents tumor cell adhesion to the body of bEnd3 cells, while Bi-joint and Tri-joint represent tumor cell

Author Manuscript Author Manuscript Author Manuscript Author Manuscript

adhesion to the junctions between two and three (or more) bEnd3 cells (see **Fig. 9a**). The number of adherent cells was counted from 5 fields of area 240 μm × 180μm in each well. Adhesion for each case was summarized for 2 wells in one experiment. The total number of adherent cells is labeled in the parentheses next to each case. Results are the mean ± SD of three independent experiments (n=3). The p value shown in each figure is from χ^2 test for the statistical test between the distribution of the adhesion location under control and that under VEGF treatment. * $p<0.05$ indicates a significant change in the number of adherent cells at the indicated locations.

Author Manuscript Author Manuscript Author Manuscript Author Manuscript

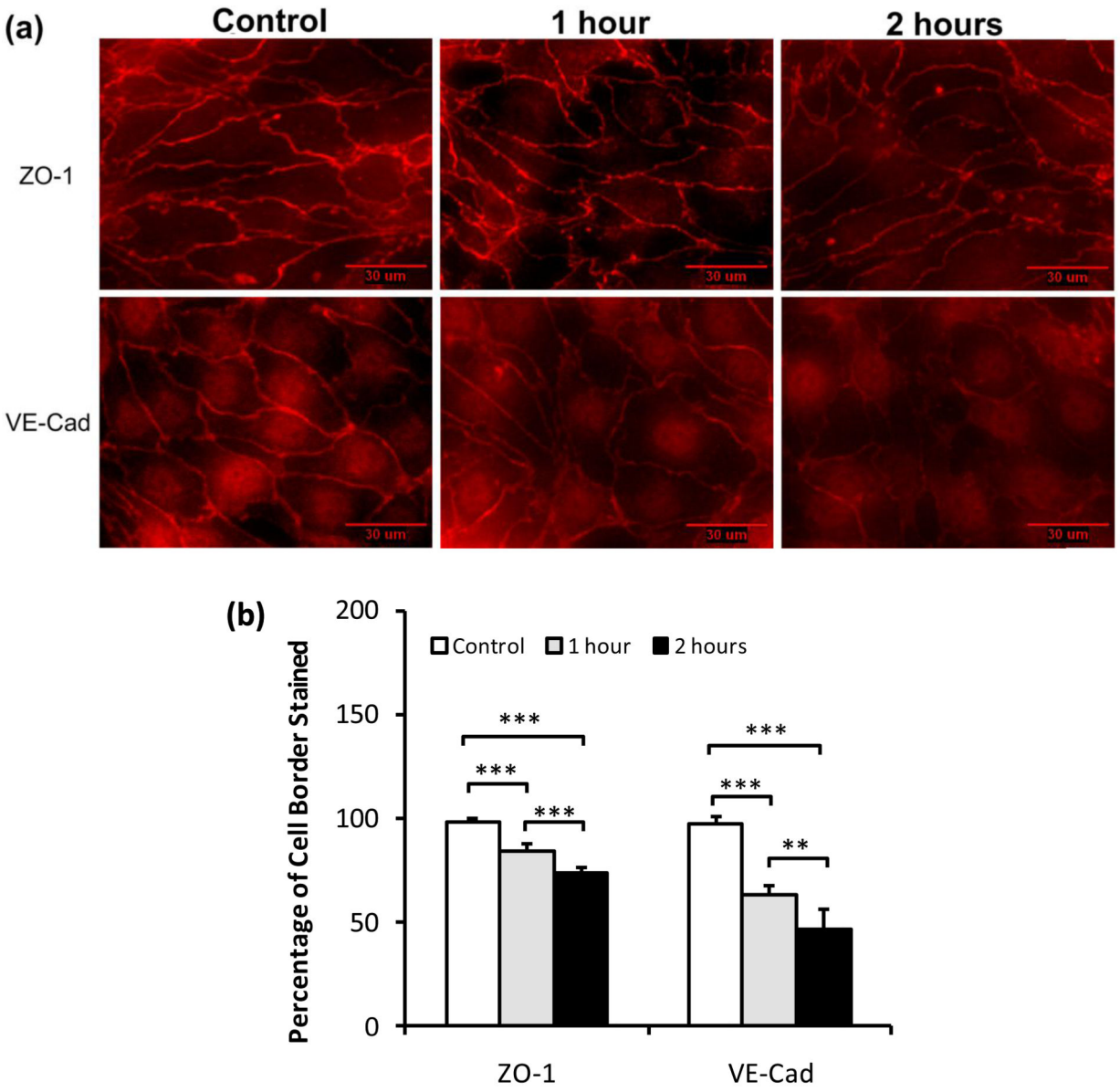

Fig.10.

Typical fluorescent images showing the effects of VEGF on bEnd3 endothelial **(a)** the tight junction protein ZO-1 (upper panel) and the adherens junction protein VE-Cadherin (lower panel) under control (1% BSA) and after 1 hr and 2hr 1nM VEGF treatment. **(b)** Junction proteins ZO-1 and VE-Cadherin were quantified by the percentage of cell border pixels having a staining intensity higher than the average intensity of the cell cytoplasm (the background) over the total cell border pixels. Ten typical fields of 120 μm × 90 μm per run for n=6 runs were analyzed. **p<0.01, ***p<0.001.

Author Manuscript Author Manuscript Author Manuscript Author Manuscript

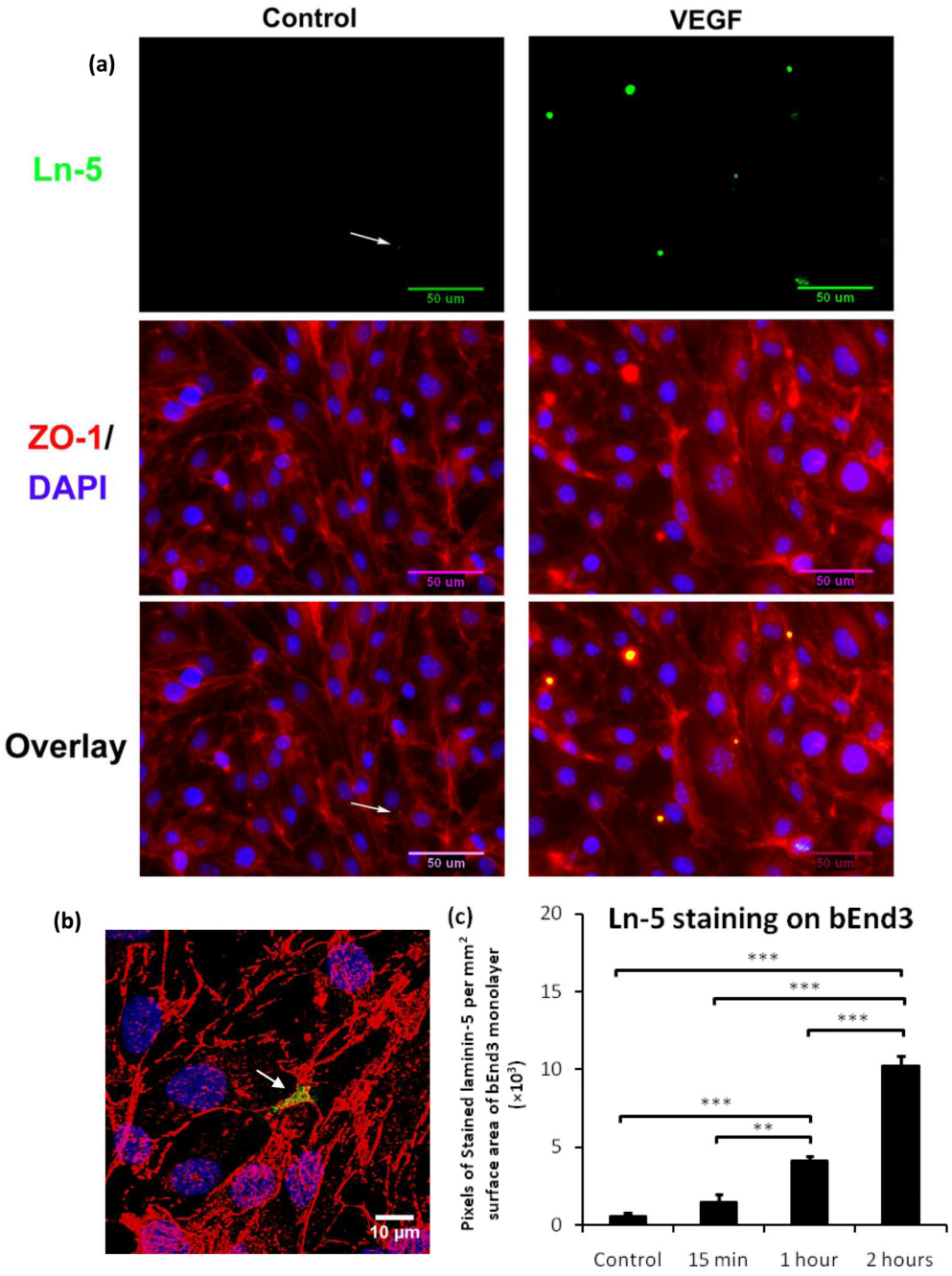

Fig.11.

(a) The upper figure is the fluorescent image showing the laminin-5 (green) at the luminal surface of the bEnd3 monolayer, which was stained before permeabilizing the cells; the middle figure shows the junction protein ZO-1 (red) and cell nuclei (blue), which were stained after permeabilizing the cells; and the bottom figure shows the overlay of the upper and middle figures, indicating that laminin-5 was located at the cell-cell junctions. The left panel shows the control result and the right panel shows staining after 1 hr VEGF treatment. The white arrows in the left panel indicate the location of laminin-5. **(b)** Confocal image of

Author Manuscript Author Manuscript Author Manuscript Author Manuscript

laminin-5 (green), ZO-1 (red) and co-localization of the laminin-5 and ZO-1 at a tri-cellular junction of the bEnd3 monolayer (the region pointed by the white arrow) after 1 hr VEGF treatment. **(c)** Comparison of the exposed laminin-5 at the luminal surface of the bEnd3 monolayer under control and after 15 min, 1hr and 2 hr VEGF treatment. Data shown is the mean ± SD from 4 runs with ten fields of 240 μm × 180 μm in each run. **p<0.01, ***p<0.001.